38. On Metal-Atom Clusters IV. Photoionization Thresholds and Multiphoton Ionization Spectra of Alkali-Metal Molecules[1])

by **André Herrmann, Samuel Leutwyler, Ernst Schumacher**[2]), and **Ludger Wöste**

Institute for Inorganic and Physical Chemistry, University of Berne, 3000 Bern 9, Switzerland

In memory of Professor *Heinrich Labhart*

(18.XI.77)

Summary

The investigation of electronic and structural parameters of metal molecules as a function of size may be decisive for understanding and control of heterogeneous catalysis with finely divided metals. Metal-atom clusters can be prepared by several methods, most of which yield a molecular mixture only. Expansion of an atomic vapour into vacuum through a supersonic nozzle creates a complex cluster-spectrum which has been investigated by photoionization using a mass-spectrometer as selective detector. Broad band single photoionization (PI.) yields the abundances and ionization thresholds for Na_x ($x \leqslant 16$), K_x ($x \leqslant 12$) and Na_xK_y ($x+y \leqslant 6$). Rough indications about other deactivation channels of excited alkali-molecules are obtained from an analysis of the photoionization efficiency (PIE.) curves. Two-photon PIE. curves with narrow-band (laser) light sources give an accurate photoionization threshold value and detailed information on ionization processes. Two-photon ionization spectra *via* a real intermediate state reached by laser excitation are equivalent to normal absorption spectra, if the excitation step is controlled by the true transition probabilities. By investigation of the power dependence of the ion current of Na_2^+ as a function of the wavelength of the tunable cw dye laser (excitation) and of the ionizing Ar^+- or Kr^+-laser, conditions under which true spectra are obtained have been clarified, in good agreement with a photon-kinetic model of the processes involved. Vibronic and rovibronic spectra of several transitions in Na_2 and K_2 have been measured. Similarly a spectrum of Na_3 has been determined mass-selectively. The scope of the new method for an absorption spectroscopy in molecular beams is discussed.

1. Introduction.[3]) – 1.1. *Metal-to-metal atom bonds* in other compounds than metallic elements or alloys have been known for many years in the Hg_2^{2+}-cation

[1]) Papers I to III of this series, see [1-3].

[2]) Author to whom correspondence should be addressed.

[3]) Abbreviations used in this communication: LN_2: liquid nitrogen; LT.: Langmuir-Taylor; QMS.: quadrupole mass spectrometer; AP.: appearance potential; IE.: ionization energy; PIE.: photoionization efficiency; TPI.: 2-photon ionization; PI.: photoionization; PIP.: photoionization potential; UHV.: ultra high vacuum.

and have recently been discovered in Cd_2^{2+} [4] and in a large number of b-metal compounds [5]. The transition metal-cluster complexes [6] comprise-2-centre and polygonal/polyhedral molecules or ions where the metal-to-metal bonded 'core' is surrounded by ligands. Well known molecular examples are polynuclear, volatile carbonyls, *e.g.* $Mn_2(CO)_{10}$, or the related species $W_2(NMe_2)_6$ [7] and $[h^5\text{-}C_5H_5Mo(CO)_3]_2$. $[Re_2Cl_8]^{2-}$, $[Re_3Cl_9L_3]$ or the $Cr_2^{II}(OCOR)_4(H_2O)_2$ units occur in lattices. The unique $Au_{11}(SCN)_3(PPh_3)_7$ [8] is a well shielded particle. Finally the 'linear metals', like *Magnus*' green salt $[Pt(NH_3)_4][PtCl_4]$ or the more recent compounds of the type $\{Pt(en)Cl_2\}$ [9] have created much interest for their anisotropic electrical conductivity and optical properties.

In most of these compounds the cluster is characterized by strong metal-to-metal atom interactions with delocalized electronic states as reflected by unusual optical, magnetic and electrical properties. The 'surface' of the clusters is occupied by ligands whose interaction with the metal atoms is of comparable strength and prevents the coagulation of many clusters to a macroscopic metallic phase.

In naked *metal molecules* $M_x(x \gtrsim 20)$ neither a lattice nor a ligand coating shield the very high reactivity of an 'unsaturated' surface. Such particles are, therefore, difficult to prepare and to study. In a way they may be regarded as thermodynamically unstable subnuclei of the solid or liquid bulk metal. If a feed of adequate activity were present for a certain time, they would rapidly grow to lose their excess surface free enthalpy and end as metallic crystals with a small ratio of the number of surface to the number of volume atoms. M_x particles must be prevented from collisions with each other. They can be created as paucidispersions or, in the limit, as monodispersions in a compartmented, unreacting environment like zeolite cages or carbon molecular sieve [10]. Normally a size distribution will be present and, unless special methods for its investigation are developed, only information about polydisperse population averages will be obtained.

Chemical interest in the preparation, characterization and properties of metal molecules has become wide-spread in recent years [12], one particular reason being that these molecules belong to a neglected domain of inorganic chemistry, the molecular chemistry of metallic elements. Most information available comes from mass-spectrometric *Knudsen*-cell measurements: Li_2, Li_3 [11] and the b-metal molecules $\leqslant Sn_7$, $\leqslant Ge_8$, $\leqslant Pb_4$, $\leqslant Bi_4$, Sn_xAu_y $(x+y \leqslant 4)$ [12] have been identified. From many metallic elements homo- or heteronuclear diatomics are known: groups Ia to Va, Ib, IIb and 3d from Sc_2 to Ni_2, furthermore Rh_2, Pd_2, Re_2, Ir_2, Pt_2, Y_2, La_2 [13].

Although mass-spectrometry yields proof of existence (*m/e*, perhaps appearance potential) and, with *Knudsen* technique, third- or second law formation enthalpies, spectroscopic information has been obtained only for Ag_3, Ag_4, (Ag_5, Ag_6?) (UV./VIS., *Raman*) [14], Ni_3 (UV./VIS.) [15], and Na_3 (ESR.) [16].

1.2. *Electronic properties* of $M_x(x \gtrsim 20)$ are expected to be quite different from metals. *Figure 1* shows HMO. eigenvalue coefficients for the 4 first body-centred regular cubic clusters M_9, M_{35}, M_{91} and M_{189} of alkali-atoms, where one *s*-valence electron/atom has been put into the molecular orbitals. This is a method which is equivalent, in the limit of an infinite lattice, to *Bloch*-waves of independent

electrons in a periodic potential with the full complement of occupied and unoccupied levels in the *s*-band. It can be recognized in *Figure 1* that small particles are *insulators* or *semiconductors* with an energy gap above the HOMO. The gap decreases with increasing cluster size and the density of states around the LUMO. becomes so high for $M_x \gtrsim 91$, that the levels cannot be drawn separately, indicating the growth of a conduction band in larger clusters (or crystal-nuclei). These circumstances are not significantly different for fcc- or icosahedral clusters.

Small-to medium-size metal molecules, *e.g.* Na_6, are *chromophores* with high oscillator strengths ($f \approx 1$) in the visible [17]. Contrary to metals, optically excited states M_x^* will have lifetimes τ adequate for the induction of photochemical reactions [18]. Discrete *ESR. spectra* are observable in odd- and in open-shell even

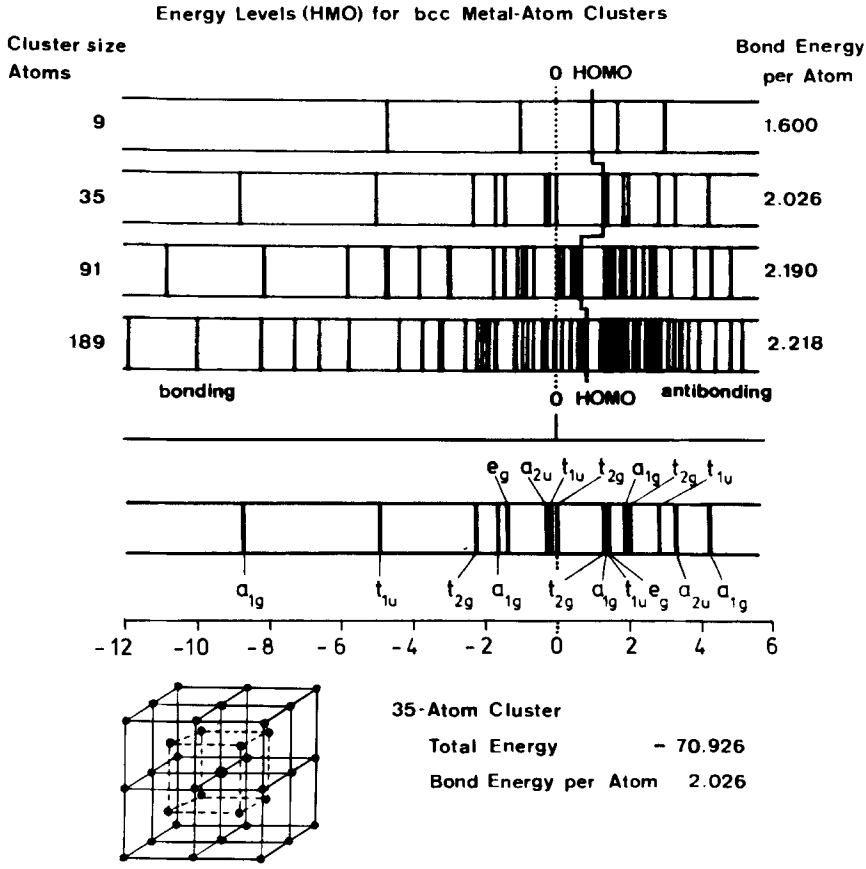

Fig. 1. *HMO.-eigenvalue coefficients of regular body-centred cubic clusters in implicit units* $(-\beta)$. At zero value the energy of an atomic Na 3*s* electron may be placed. The upper part gives the level schemes for the first 4 clusters. HOMO. is the highest occupied MO. of the ground state. The asymptotic progression of the lowest a_{1g} level is recognizable as well as that of the bond energy per atom. β could be calibrated at the asymptotic bond energy of the bulk phase. The lower part gives a view of the 35-atom bcc-cluster together with an indication of the symmetry species of each HMO. level

M_x-molecules [16] [17], with a rapidly growing number of transitions of smaller and smaller intensity as x increases.

1.3. *Structural differences* in M_x against M_∞ are known in general [19]. The diatomics have between 10–20% smaller atomic distances than the bulk metal, indicating an effect of 'surface tension'. If this is a dominant factor in M_x molecules with sizes up to crystal-nuclei, different equilibrium symmetries from the bulk may be formed. Icosahedral shapes with five-fold rotational symmetry have been observed [20] and *Bagley, Hoare & Pal,* and *Burton* [21] have described their crystal structure as five-fold twins with close packed surfaces of ~(111) planes. The series M_{13}, M_{55}, M_{147}, M_{309}, $M_{561...}$ of body-centred icosahedra has a larger relative number of surface atoms than bcc- or fcc-clusters with (100) planes of an equal number of atoms. Nevertheless, their surface area is smaller than for equivalent cubic clusters up to a size of ~23000 atoms (for the infinite bulk it is 2.7% larger, and icosahedra are unstable). In fact, small icosahedra offer a minimum surface (short of a sphere) compatible with a twinned close-packed regular lattice. The M_{10179} bc icosahedron has still 19.3% of its atoms in the surface layer. M_x molecules with $x \neq$ bcc, fcc or icosahedral regular polyhedra will have surfaces and structures not found in ideal bulk crystals. They will imitate most, if not all, types of convex surface defects believed to be responsible for the catalytic activity of finely divided metals. Paucidispersions of M_{10}–M_{15} might, for example, offer an almost 100% active catalytic surface for certain processes. Effects of this nature have been observed [22] [23] and speculated upon [24].

1.4. *The preparative methods* for the syntheses of metal molecules are in a primitive state. It is, of course, much more demanding and subtle to create molecules than metal atoms, a technique well advanced recently by the work of *Timms* [25] and others. Co-deposition of rare gases together with a monoatomic metal vapour on a cold target at ~10° K, *e.g.* sapphire-windows, leads to: 1) *matrix isolation of metal atoms* if conditions are chosen carefully [26]. If the co-deposition is made with a controlled temperature gradient within the matrix, or the matrix is slightly warmed, matrix sites relax and metal atoms diffuse slowly, thus meeting each other and forming diatomics at low, and larger molecules at high, metal-atom concentrations. In order to create M_5 to M_6 the metal-atom concentrations must be as high as one metal atom on 20 Kr atoms, which means that every second to third neighbour in the consensate is another metal atom. A slight disturbance of this system causes spontaneous reaction to macroscopic crystals [13] [14]. With present techniques, larger molecules will not be accessible by this method. 2) Another type of matrix isolation is the creation of clusters within the *pore structure of molecular sieves.* Metal cations located in the pores as counterions of the aluminosilicate framework may be reduced by hydrogen [10] or photochemically [18][1]). Cluster condensation from a metal vapour into the molecular sieve is also feasible [17]. Contrary to the rare gas matrix isolated molecules, a study of their chemical reactivity and other properties is easily possible in molecular sieves since the

---

[1]) *Note added in proof:* Ag_4^{3+} clusters have been identified in molecular sieves by X-ray analysis, *Y. Kim & K. Seff,* J. Amer. chem. Soc. *99*, 7055 (1977).

system remains as created at temperatures even well above 300° K, where ordinary matrices are not existent. This form of cluster containment is, of course, a well known industrial process used for making zeolite-supported metal catalysts [10]. The role of the clusters, their structure and electronic properties are, however, not well understood. 3) Only the formation of *gaseous metal molecules*, with the proper techniques to investigate them, would yield information about the unperturbed particles. In *Knudsen* cells, vapour and condensed phase(s) are in thermal equilibrium. The effusing hot vapour contains larger molecules, if they are present within the cell. Higher clusters of real metals have not been found with this technique [11].

Effusion under pressure/temperature- and aerodynamic conditions proper for the formation of a supersonic jet, however, produces a dramatic depletion of the internal kinetic energy of the viscous vapour so that, at the boundary to molecular flow conditions, a very cold gas creates a whole spectrum of small to large clusters [27]. Since this technique leads to intense molecular beams, all the well advanced tools for beam-diagnostics are available for the investigation of the particles. We have adapted and developed this technique. A few more preparative schemes are promising: 4) *thermal, photochemical or reactive ligand-stripping of (transition)metal-cluster complexes.* Uranocene can be stripped from the cyclooctatetraene ligands by collisions with metastable $^3P_{0,1,2}$ rare gas atoms [28], yielding cold U-atoms. Similarly, polynuclear transition metal carbonyls can be stripped to the naked, cold metal clusters [29]. 5) *Electron impact fragmentation* of transition-metal cluster complexes leads to atoms and naked clusters [30]. 6) Evaporation from an oven into a rare gas at $\sim$10 Torr *(collisional condensation)* has led to large Li_x-clusters [31]; 7) *sputtering techniques* give condensates of varying particle sizes among which small molecules might exist [32].

More preparative schemes exist beyond the seven types mentioned and will be tested. For the investigation of clusters, processes other than those used for chemical or catalytic reactions are more suitable. We concentrate henceforth on gaseous metal molecules.

1.5. *The characterization of metal molecules* in a polydisperse system, that is a molecular mixture, depends on the availability of particle-specific methods. For gaseous mixtures in a collision-free environment, the mass-spectrometer is a highly sensitive instrument with *m/e*-specificity. With common MS. techniques *m/e* values, fragmentation patterns and, with special equipment, appearance potentials and the observation of decay processes of excited particles are secured. Because the electronic states and gyrovibrational transitions of metal molecules are of paramount interest, optical spectra are needed as well. A combination of absorption spectroscopy with MS. can yield this information: a narrow band light source provides selective excitation of molecules followed by photoionization of the excited state with a second light source and mass-selective detection in the MS., hence perfect particle-specificity of the process. If now the exciting light source is a tunable (dye-) laser of satisfactory band width, and the 2-photon sequence is made excitation controlled, the recorded ion-current as a function of wavelength is the correct absorption spectrum of the mass-selected species. With the sensitivity

of mass spectral detection devices an absorption spectroscopy from near UV. to near IR. of multiparticle molecular beams has for the first time been realized.

This paper presents the methodology for the preparation and investigation of metal molecules we have developed in the past 2 years, exemplified by the investigations of alkali-metal molecules, but not limited to them.

2. Apparatus. – 2.1. *The molecular beam apparatus* is shown in *Figure 2.* It consists of a 3-stage differentially pumped vacuum system: an oven chamber, a collimator chamber and an observation chamber [33]. The system is designed with high-vacuum technology, constructed of V4a stainless steel with *Viton* O-ring seals. Each chamber is pumped with a 1000 l/s oil diffusion pump (*Leybodiff* 1000) baffled with a LN_2 cooled trap. A by-pass system, mainly consisting of two VAT, flatvalves, allows the oven chamber to be flooded separately for a quick service. The diffusion pump is filled with *Diffilen* Oil. Silicon oil tended to polymerize in the presence of alkali vapour. The pump is connected to a 30 m^3/h roughing pump (*Alcatel* 2030). In the other diffusion pumps silicon oil (DC 705) did not cause problems. They are each connected to a 12 m^3/h roughing pump (*Alcatel* 2012). Three *Leybold Combitron* systems – using ionization and *Pirani* gauges – provide the vacuum measurement and control. The vacuum measured with the oven switched on was 10^{-4} Torr in the oven chamber, 10^{-6} Torr in the collimation chamber and 10^{-7} Torr in the observation chamber.

The oven system, shown in *Figure 3*, is designed as an interchangeable cartridge system, so that different nozzles could easily be investigated. The nozzles were drilled by *G. Frey KG*, Berlin. Optimum performance was found for a nozzle of 0.2 mm diameter and 0.4 mm channel length. The prepared nozzle is welded off axis onto the cartridge. This allows the oven to be filled to 80% of its volume (30 ml) which usually lasts for an 8 h run. Na and K are high purity grade. K is distilled 3 times *in vacuo* prior to use. It is simpler, however, to use liquid NaK and extract paraffin residues with heptane. The cartridge is filled in pure dry N_2, then sealed with a thin Ta or Mo sheet pressed against a tempered Cu disk.

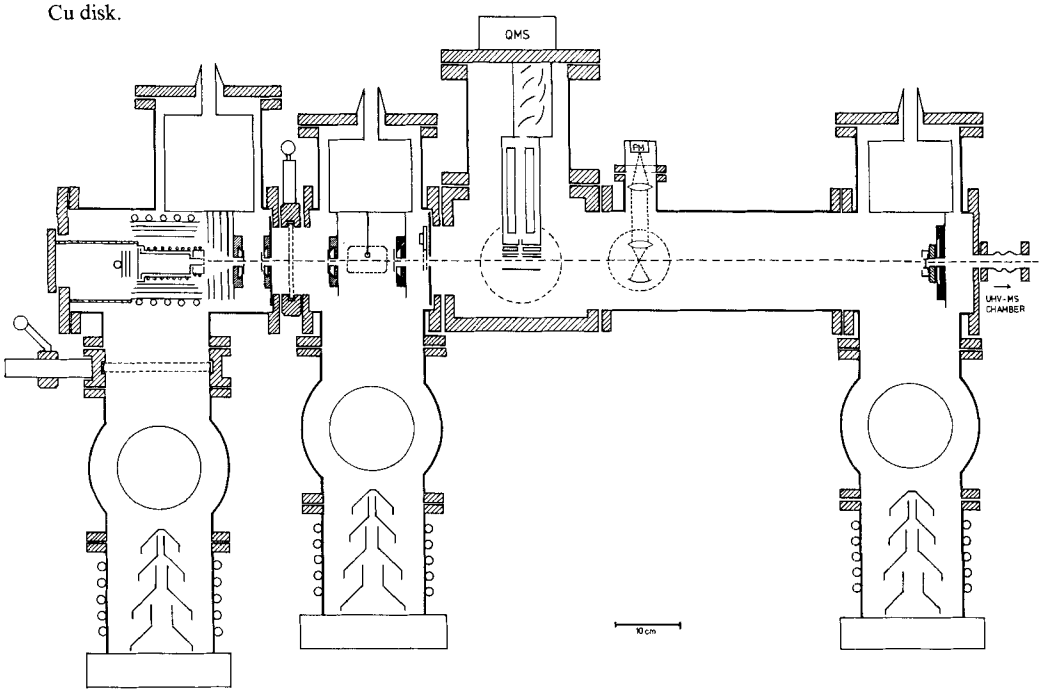

Fig. 2. *Molecular beam apparatus consisting of a 3-stage differentially pumped vacuum system:* the oven chamber, the collimator chamber and the observation chamber, in which the quadrupole mass-spectrometer is placed

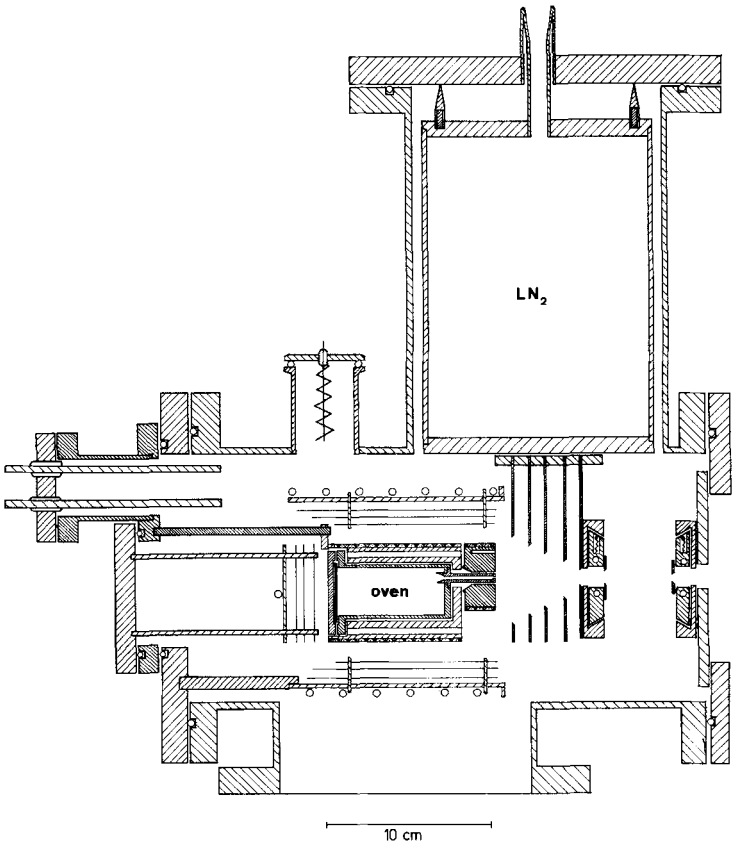

Fig. 3. *Vertical section through the oven part which is designed as an interchangeable cartridge system.* Collimators are suspended from an LN_2-cooled trap

Oven and nozzle are independently heated with thermocoax heating wires, which are directly welded onto a heating jacket, and their temperatures are measured with Chromel/Alumel thermocouples. The arrangement is shielded with a 3-fold Ta jacket inside a water cooled cylinder. Temperatures up to 1100°C were achieved. A set of 6 LN_2 cooled collimators of chrome plated copper with diameters decreasing from 60 to 4 mm is used for rough collimation and trapping vagabonding particles, which completely avoids a contamination of the oven chamber. Two further collimators of 2 and 1 mm diameter, which easily clog, can be adjusted and exchanged with linear motion feedthroughs (VG LM50) from the outside.

The second chamber contains 2 more LN_2-cooled banks with 6 slits each for a fine beam collimation. Slit widths are 0.02, 0.05, 0.1, 0.2, 0.5 and 1 mm. They also can be exchanged and adjusted from the outside. The beam is passed through a high voltage condensor to extract ions formed in the expansion area.

Furthermore, the collimation chamber contains a 400 Hz *Bulova* tuning-fork chopper, to chop the beam for phase sensitive detection. In this way beam components are completely separated from vacuum background during mass-spectrometric detection. There was, for example, no problem in detecting Na_6 at *m/e* 138 when a considerably stronger Ba background peak was present. The tuning fork chopper is also adjusted from the outside. It is softly suspended on rubber-bearings to prevent microphonic transmission to the multiplier system.

A quadrupole mass-spectrometer (Extranuclear 270-9/ELFS) placed vertically in the observation chamber is used as a mass-sensitive beam analyser. The ion source was modified for photoion collection by replacing the cathode plate with a repeller plate fixed at 15 mm distance from the ion entrance, and kept at the 'ion region'-voltage. The molecular beam and the ionizing light is passed at right angles between the ion entrance and repeller plate. To prevent photoelectron formation, special care is taken that no light touches metal parts near the ion source. It is passed through window flanges on both sides of the ion source.

Further window flanges are used for laser-induced fluorescence experiments [34]. Special optical components image the beam fluorescence on a photomultiplier tube (RCA 7265). Phase-sensitive detection of a chopped molecular beam proved to be very useful for fluorescence experiments as well, since it eliminates all background arising from scattered light.

The total beam flux is monitored with a *Langmuir-Taylor* surface ionization detector, which can be moved perpendicularly to the beam for measuring the beam profile. The LT.-detector can be used to measure absolute photoionization efficiences by the decrease of signal when the ionizing light is switched on. It serves also for measuring the molecular beam deflection induced by the total photon momentum [35], which is very useful for the determination of absolute excitation efficiencies. For mass-selective photon-momentum spectroscopy, the molecular beam apparatus can be connected with a UHV.-MS. chamber. So far we have been able to achieve well resolved spectra of the Na_2 $A \leftarrow X$ system by photon-momentum spectroscopy [36].

2.2. *The appearance potentials* of the alkali aggregates were measured with the following apparatus *(Fig. 4)*: The light of a 1 kW Hg-lamp (*Oriel* Model 6242) was passed through a modified *Spex Minimate* illumination monochromator and focused at right angles onto the molecular beam using a 150 mm focal length fused silica lens [37]. The spectral light intensity was simultaneously measured with a bolometer and the total beam intensity was controlled with the LT.-detector. For ion currents $> 10^{-15}$ amps a PAR lock-in system 186A/181 was used, while smaller currents were counted with a *Brookdeal* 5Cl digital lock-in amplifier, switched on-line with a HP 9830 calculator. The measurements were performed by keeping the mass spectrometer on a fixed *m/e*, while the wavelength of the illumination monochromator was scanned. For clusters $M_x (x > 8)$ the monochromator was replaced by direct lamp irradiation, filtered with a set of 24 UV. cut-off filters in 5 nm steps (*Schott & Co.*, Mainz).

2.3. *The two-photon ionization experiment* was performed with two light sources *(Fig. 5)*: A cw dye laser serves as exciting light source, and an Ar^+-laser (CR 12), a Kr^+-laser (SP 171), a second dye laser

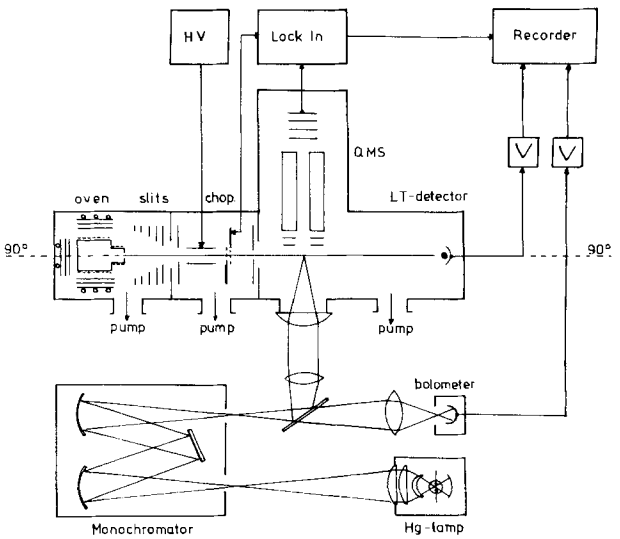

Fig. 4. *Scheme of the PI. experiment with molecular beam apparatus, Hg lamp, monochromator assembly and recording units*

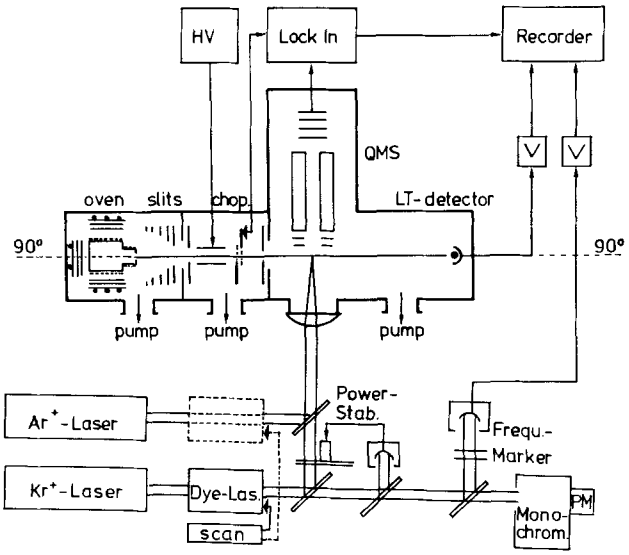

Fig. 5. *Scheme of the TPI. experiment showing the light pass of the exciting laser and the ionizing laser.* A monochromator is used for the determination of the dye laser wavelength. The Hg-lamp (not shown here) is focused into the molecular beam through an opposite window flange

or the Hg lamp as ionizing light source. The lasers are focused into the interaction region with a 300 mm focal length cylindrical lens. The wavelength of the dye laser is measured with a *Spex 1870* monochromator, which is calibrated with a Ne spectral lamp. The laser band-width is measured with a *Fabry-Pérot* etalon, which also serves as a frequency marker for scan control. Since changing the laser pump power may change its bandwidth or mode structure, the laser power is monitored with a thermal disc and externally power-stabilized with a servo-controlled variable beam splitter.

2.4. *The laser* required for the spectroscopic concept had to be continuous with a wide tuning range and high stability. Jet stream dye lasers offer a tuning range from 965 to 407 nm. But because of their unsatisfactory stability, we developed an improved jet laser system.

The main frequency fluctuations in jet lasers result from thickness fluctuations in the active region [38], so the whole laser arrangement is mounted on a 2 tons marble plate (*Poschiavo* serpentine) suspended in a sand box on air bags and styrofoam cushion to protect it from external vibrations.

Special care was also taken in the design of the pumping system and the nozzle. The dye solution is circulated with a high performance centrifugal pump or gear pump. It is passed through a heat exchanger, a Millipore filter (1μ) and a buffer volume. Pressures are set with a by-pass line. The nozzle is made of 2 precisely machined parallel plates 0.2–0.4 mm apart (*Troller AG*, Murgenthal) with a sharp cut-off corner, forming a homogeneous flow channel of rectangular profile. Typical flow velocities are 15 m/s.

Usually ethylene glycol is used as a solvent in jet stream dye lasers. The thermooptical properties of ethylene glycol (specific heat constant and dn/dT) cause serious 'schlieren' effects in the active region, however. These values are considerably more favourable for water solutions. Therefore, we use water dye solutions with viscosity-raising additives like polyvinylalcohol. Thus the stability of our laser could be improved by a factor of 5. The optimum bandwidth we achieve in single mode operation is 5.5 MHz [39].

Usually we employ the folded 3-mirror cavity (*Kogelnik* configuration, *Fig. 6*) which has very low losses and good tuning properties [40]; the light of the pump laser is focused into the jet, where the mirrors M_1, M_2 and M_3 form a resonator around the fluorescent spot. M_1 and M_2 are high reflectance mirrors (curvature 5 and 7.5 cm for RH 6G), the flat mirror M_3 being used as output coupler (transmission between 4 and 15% depending on gain). The laser wavelength is set with a 3-plate birefringent

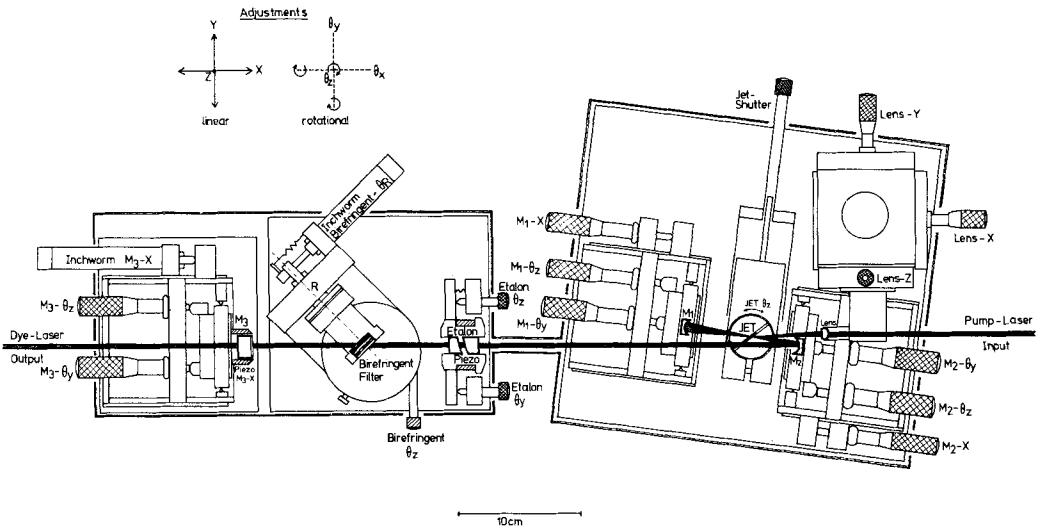

Fig. 6. *Jet stream dye laser system in* Kogelnik *configuration.* The light of the pump laser is focused with a lens onto the free-running jet. The mirrors M_1, M_2, and M_3 form the laser cavity. Wavelengths are set with the birefringent filter and the etalon (optional)

filter *(Coherent Radiation)* [41]. Single mode operation is achieved with an etalon (SP Model 581A) inserted in the cavity [42]. For large wavelength scans (1 Å $< \Delta\lambda <$ 1000 Å) no etalon is used, however, resulting in 0.5 cm^{-1} laser bandwidth determined by the dispersion curve of the birefringent filter *(Fig. 7)*. In this case, a high-resolution spectrum of the laser output shows a number of equidistant discrete lines, the longitudinal resonator modes. To avoid this and to obtain a quasihomogeneously broadened laser output spectrum, a 10 kHz wobble signal is applied to the output mirror piezo.

The concept of the laser design was to keep all adjustments independent from each other *(Fig. 6);* the pump laser focusing element is therefore adjusted with an XYZ-translator (Micro-Contrôle MR80). The nozzle is held in a cylindrical mount allowing adjustment of the *Brewster* angle. The curved mirrors M_1 and M_2 are positioned in the centre of the cardanic angular orientiation device (*Lansing* 10.203) mounted on a linear translation stage (*Lansing* 20.124) for adjusting the focus.

The birefringent filter, fixed on two rotational elements (Micro-Contrôle TR80) can be adjusted on the wavelength axis, R, and the *Brewster* angle. Wavelength scans are performed with an Inchworm Translator (*Burleigh* PZ500). A Kr^+-laser and an Ar^+-laser are used as pump lasers, or alternatively as ionization light sources.

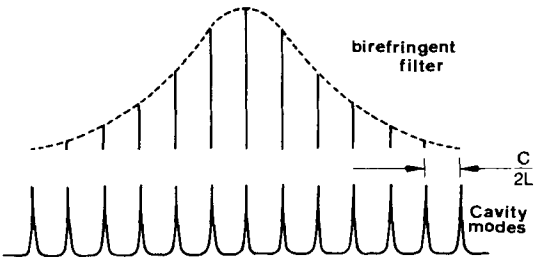

Fig. 7. *Longitudinal modes of the dye laser, operated only with birefringent filter as dispersive element.* To achieve a '*quasi*-homogeneously' broadened laser output, a 10 kHz wobble signal is applied to the output mirror M_3-piezo (see *Fig. 6*)

3. Broad band photoionization. - 3.1. *Electron impact ionization/photoionization.* The first attempt to ionize Na clusters produced in a supersonic beam with low-energy electrons was partially unsuccessful, the largest cluster observed being the trimer. The electron ionization efficiency curves *(Fig. 8)* show clearly that the trimer is fragmented by electrons of more than about 20 eV energy. The observation of dimers at electron energies far higher than needed for dissociation may be due to ionization of low lying core levels. Higher Na_x species are not detectable because they have even more fragmentation channels available than the dimer and are, therefore, destroyed.

To overcome this destructive effect of electron-ionization we use the photoionization (PI.) technique [27]. The light source is a high pressure Hg lamp with a power of 1 kW. The maximum photon energy obtainable is about 6 eV, corresponding to 206 nm. With this lamp directly focused into the beam we could observe the existence of the complete series of aggregates up to Na_{16} and K_{12} [1]. *Figure 9* reproduces the mass spectrum from Na to Na_8 obtained with a single mass-scan. The intensities are not corrected for the different discriminating factors but the concentration of Na_3 in the beam appears to be about 100 times less than that of Na_2. The intensity pattern is not really significant as a characterization of the clusters, not only for the reasons mentioned, but especially because the formation of aggregates through expansion is a non-equilibrium process.

3.2. *Appearance potentials.* The measurement of an intrinsic property of these clusters for comparison throughout the whole series is of great importance. The easiest one obtainable so far is the ionization energy (IE.).

For this purpose (see *Fig. 4*) we inserted a monochromator between the lamp and the beam to select photons of variable energies whose dispersion depends on the grating and the input and output slits of the monochromator. *Figure 10* shows the discrete lamp spectrum in the region of interest and the corresponding broadened spectral function resulting from a convolution with the slit function of the monochromator.

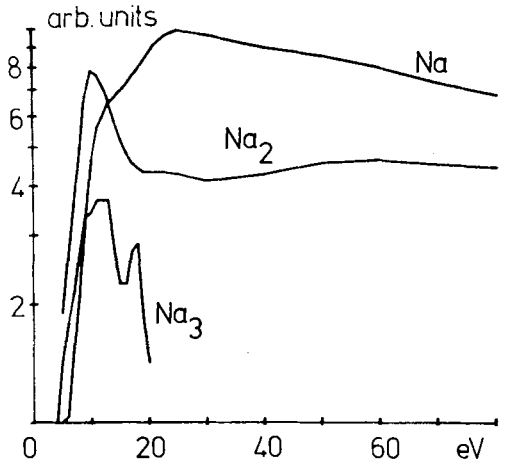

Fig. 8. *Ionization efficiency for Na, Na_2 and Na_3 vs. electron energy for electron impact*

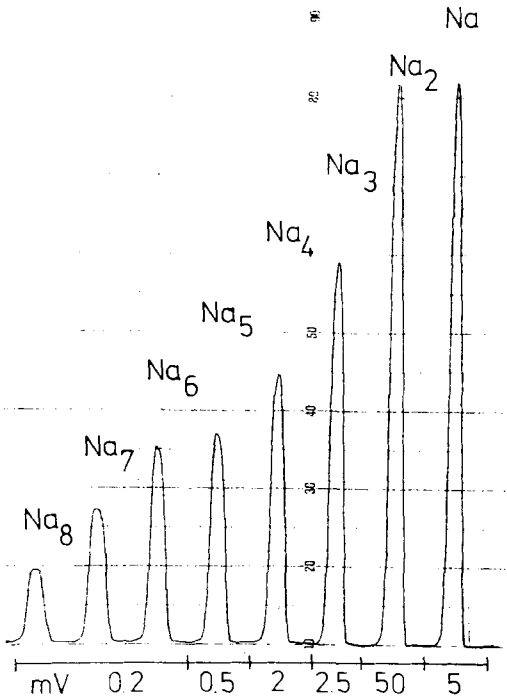

Fig. 9. *Single-scan MS. of a Na supersonic nozzle-beam, using photoionization.* The different sensitivity ranges of the recorder are indicated

The QMS. is set at a desired *m/e* and the ion intensity is measured while continuously varying the wavelength of the impinging photons. A set of the curves obtained is presented in *Figure 11*. One notices immediately that Na_3^+ is still measurable at wavelengths where Na_2^+ signals no longer exist, *i.e.* Na_3 has a lower IE. than Na_2. The problem is now to determine exactly the respective threshold energies.

Many publications treat this subject (*cf.* [43]), but the spectral emissivity of the lamp, which influences drastically the whole appearance of the curves, has never been taken into account. The measured ion intensity $C_x^+(\lambda_0)$ of cluster M_x at wavelength λ_0 is given by

$$C_x^+(\lambda_0) = \int_{-\infty}^{\infty} F_x(\lambda) \cdot M(\lambda_0 - \lambda)\, d\lambda \tag{1}$$

where $M(\lambda_0 - \lambda) = -M(\lambda - \lambda_0)$ is the monochromator function, and $F_x(\lambda) = L(\lambda) * P_x(\lambda)$ is the product of $L(\lambda)$ the number of photons with energy hc/λ emitted by the lamp between λ and $\lambda + d\lambda$ with $P_x(\lambda)$ their relative photoionization efficiency (PIE.) for M_x to be determined.

This expression represents a convolution of the 2 functions $F_x(\lambda)$, $M(\lambda_0 - \lambda)$ and is easy to handle by discrete *Fourier* transformation:

$$\mathcal{F}(C_x^+) = \mathcal{F}(F_x) \cdot \mathcal{F}(M) \tag{2}$$

The monochromator function is derived from the measured Na atom ion-yield curve $C_1^+(\lambda)$ whose PIE. curve is set equal to 1 for $\lambda < 241$ nm, $\frac{1}{2}$ for $\lambda = 241$, and 0 for $\lambda > 241$ nm; $P_1(\lambda)$ is a unit step function at 241 nm (5.14 eV).

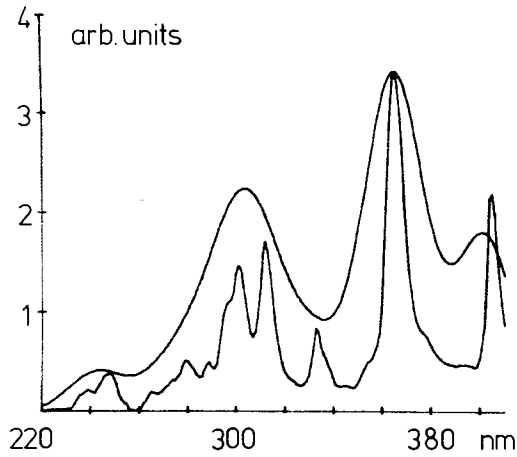

Fig. 10. *1 kW high-pressure Hg-lamp spectrum and the curve resulting by convolution with the slit function of the monochromator*

The monochromator function found is nearly gaussian and can now be applied in eq. (2) to determine $F_x(\lambda)$, and hence $P_x(\lambda)$.

In another approach, we assume that the PIE. curve for the higher clusters is also a unit step function, calculate a theoretical $C_x^+(\lambda_0)$ curve for different thresholds, and fit it to the measured one.

Both methods lead to very satisfactory comparisons as shown in *Figure 12*. The measured photoionization energies so obtained are summarized in *Table 1*.

The graphical representations (*Fig. 13* and *14*) are more explicit for comparisons in the series, from which we can observe the following: 1. In going from Na_2 (K_2) to Na_3 (K_3) there is a jump of about 1 eV (0.76 eV); such a large difference does not occur again in the Na_x, K_x series; 2. The odd aggregates up to

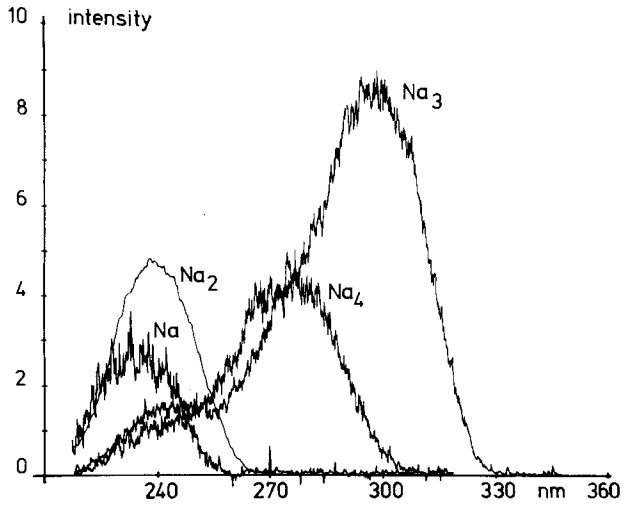

Fig. 11. *Measured PIE. curves* vs. *wavelength for the first Na_x molecules*

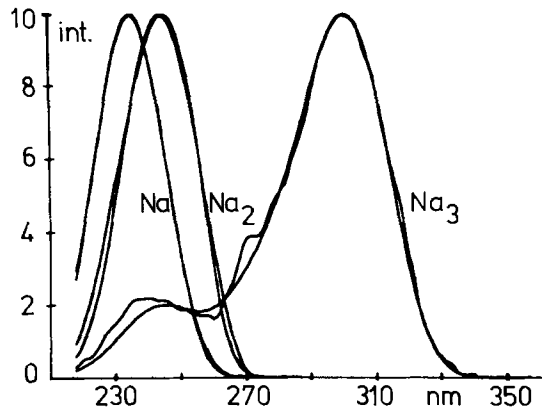

Fig. 12. *Comparison between calculated (see text) and measured PIE. curves*

Na_9 are easier to ionize than the even ones, suggesting the paired electrons to be more strongly bonded than the unpaired ones; 3. The values for Na_x tend slowly towards the bulk workfunction (2.3 eV).

The ionization energy of the mixed clusters seems to be a simple combination of the ionization energy of the corresponding homonuclear species. The appearance potential (AP.) of the heteronuclear cluster M_nV_t can be found with the rule

$$AP.(M_nV_t) = \frac{n}{n+t} AP.(M_{n+t}) + \frac{t}{n+t} AP.(V_{n+t}) \qquad (3)$$

Table 1. *PI. threshold energies for alkali clusters (eV)*

	Prior Values[a])	This Work [1]		Prior Values[a])	This Work [1]
Na	(5.14)[b])	(5.14)	K	(4.34)	(4.34)
Na_2	4.9 ±0.1	4.934±0.011[e])	K_2	4.0±0.1	4.05 ±0.05
		4.866±0.014[c])			4.059±0.001[d])
Na_3	3.9 ±0.1	3.97 ±0.05	K_3	3.4±0.1	3.3 ±0.1
Na_4	4.2 ±0.1	4.27 ±0.05	K_4	3.6±0.1	3.6 ±0.1
Na_5	3.9 −4.3	4.05 ±0.05	K_5		3.3 ±0.1
Na_6	4.05−4.35	4.12 ±0.05	K_6		-
Na_7	3.9 −4.15	4.04 ±0.05	K_7		3.3 ±0.1
Na_8	4.0 ±0.1	4.10 ±0.05	K_8		3.4 ±0.1
Na_9		4.0 ±0.1	NaK	4.5±0.1	4.52 ±0.05
Na_{10}		3.9 ±0.1	Na_2K	3.6±0.1	3.7 ±0.1
Na_{11}		3.8 ±0.1	Na_3K		4.1 ±0.05
Na_{12}		3.6 ±0.1	Na_4K		4.0 ±0.1
Na_{13}		3.6 ±0.1	Na_5K		4.1 ±0.1
Na_{14}		3.5 ±0.1	NaK_2	3.4±0.1	3.6 ±0.1
			Na_2K_2	4.1±0.1	4.0 ±0.1

[a]) *E. J. Robbins, R. E. Leckenby & P. Willis,* Adv. Physics *16*, 739 (1967), and *P. J. Foster, R. E. Leckenby & E. J. Robbins,* J. Physics *B2*, 478 (1969).

[b]) In brackets: calibration values.

[c]) Determined by TPI. *via* $A^1\Sigma_u^+$ ($v' = 6,8,11,13$), 9 measurements with laser and monochromator.

[d]) Determined by TPI. *via* $B^1\Pi_u$ ($v' = 1$ to 10) 10 measurements with two lasers.

[e]) 12 independent monochromator measurements.

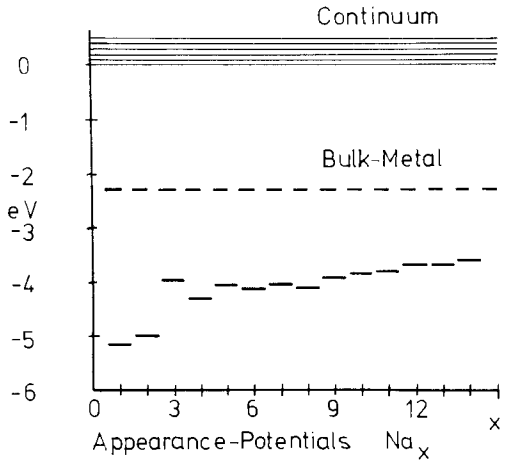

Fig. 13. *PI. threshold energies for the series of Na_x molecules from $x=1$ to 14.* The dashed line indicates the work function of the bulk metal

where AP.(M_{n+t}) and AP.(V_{n+t}) are the AP. of the homonuclear parents. *Table 2* compares measured and interpolated values for the 6 available heteronuclear clusters.

The mean of the absolute difference is $|\bar{\Delta x}| = 0.051$ eV with a standard deviation $\sigma = 0.0324$. This rule seems to be well applicable as long as the precision of the data used is good. It serves, for example, to estimate Li_x ionization potentials from measurements of the Na_xLi_y AP.

3.3. *The threshold step.* For almost all the measured clusters the pre-threshold and threshold parts of the experimental and fitted curves overlap very well, hence the unit step function for $P_x(\lambda)$ appears to be an acceptable approximation. In fact $P_x(\lambda)$ depends on several parameters: the internal thermal energy distribution

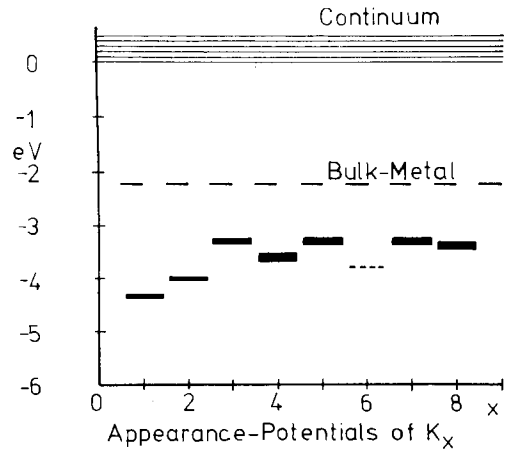

Fig. 14. *PI. threshold energies for K_x molecules containing up to 8 atoms.* Precision is indicated by the thickness of the horizontal bars. The K_6 value is uncertain

Table 2. *Comparison between interpolated (eq. (3)) and measured PI. threshold energies*

	Composition		Interpolated (eq. (3))	Measured
NaK	1/2 Na_2	+ 1/2 K_2	4.497 ± 0.006	4.52 ± 0.05
Na_2K	2/3 Na_3	+ 1/3 K_3	3.75 ± 0.1	3.7 ± 0.1
Na_3K	3/4 Na_4	+ 1/4 K_4	4.10 ± 0.06	4.1 ± 0.05
Na_4K	4/5 Na_5	+ 1/5 K_5	3.90 ± 0.06	4.0 ± 0.1
NaK_2	1/3 Na_3	+ 2/3 K_3	3.52 ± 0.08	3.6 ± 0.1
Na_2K_2	1/2 Na_4	+ 1/2 K_4	3.94 ± 0.08	4.0 ± 0.1

in the ground state of the neutral rotor and oscillator, the related *Franck-Condon* factors for transitions to ion states, the transition probabilities to *Rydberg* states and their autoionization probabilities, the singlet-doublet complication of ionization *etc.* [43].

We have observed ([2] and section 4) that at least the dimers are very cold: vibrational temperatures of < 100°K, and rotational temperature < 40° K are found, so that $> 90\%$ of the dimers are in the $v'' = 0$ state, and less than 1% have $v'' = 2$. For this reason and because the energy range near threshold is very small, a step function is a good approximation, well supported within the experimental precision and resolution of the monochromator.

3.4. *Information about other processes.* Processes in the post-threshold region are more complex. First it is not realistic to assume that $P_x(\lambda)$ remains constant over a large λ-region; secondly at higher photon energy other deactivation channels become active, among which fragmentation, dissociation to ion pairs, dissociative ionization, indirect ionizations *via Rydberg* levels are important. This last ionization process has been observed in the form of autoionization lines for K_2^+ using an intense flux of quasi-monoenergetic photons (see section 4). In spite of these indirect channels for ionization, no marked discrepancies from the ideal unit step are found using the Hg lamp and monochromator *(Fig. 12)*. This is due to the fact that the photons at any one nominal λ_0 have a broad energy distribution exciting many of these transitions at the same time. The resulting measured smooth signal corresponds to the convolution of the monochromator window with the discrete ion spectrum.

For Na_3 the calculated curve for a threshold value of 3.97 eV is in good agreement with the measured signal even in the post-threshold region. For all the higher species the calculated intensities for the post-threshold region are higher or lower than measured. A remarkable alternance exists: for Na_4, Na_6, Na_8 the fitted PIE. curves are too high at smaller λ and for Na_5, Na_7 they are too low *(Fig. 15–19)*. This may be related to the stability of the ions: for $Na_{n>3}^+$ the odd-cluster ions are more stable than the even ones. There is agreement with the conclusion of *Leleyter* about the relative Li_n^+ intensities formed by secondary ion emission [44] and with the fact that the odd electron is in an antibonding MO.

Heteronuclear dimers are of great interest because they have a ground state dipole moment. Vibrational cooling by IR. emission is therefore electric-dipole allowed, hence they may be colder in the downstream beam than the homonuclear dimers. The heteronuclear ions are known to be less stable than their neutral form contrary to the homonuclear species [1]. Fragmentation may therefore be observable in the accessible energy range. Indeed it was not possible with our simplified ionization model to calculate satisfactory NaK ionization efficiency curves beyond the threshold. *Figure 20* shows the measured and calculated NaK^+ curves for an ionization threshold of 4.52 eV, together with the intensity difference between the 2 curves. Taking into account the shift of the toe of the curve due to the monochromator function one obtains 4.92 eV (252 nm) as threshold energy for a process competitive with direct ionization.

A possible channel which fits well is the following:

$$NaK^* \rightarrow Na + K^+ + e^- \qquad 4.96 \text{ eV (adiabatic)}$$

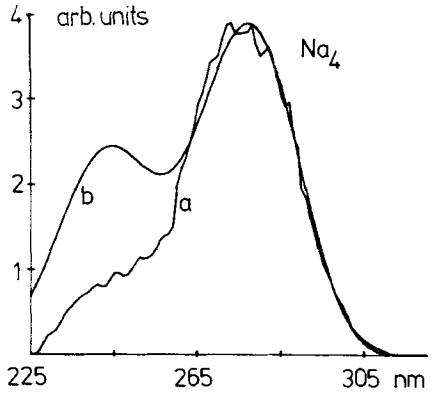

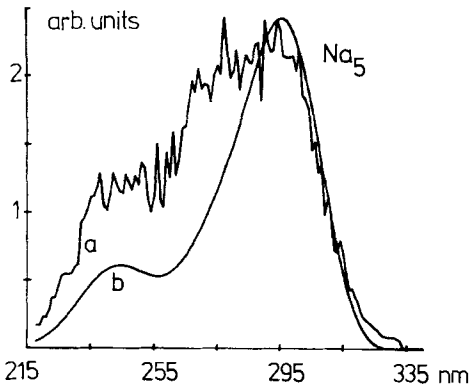

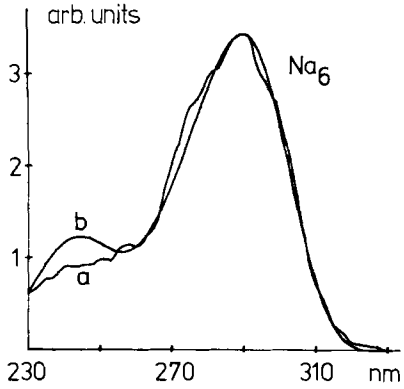

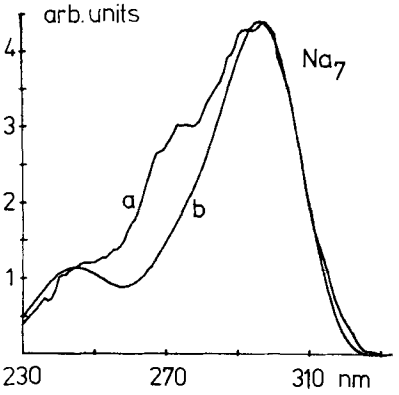

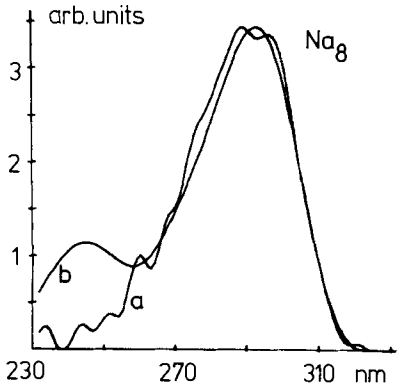

Figs. 15–19.
Comparison between a) measured and b) calculated PIE. curves
(see text)

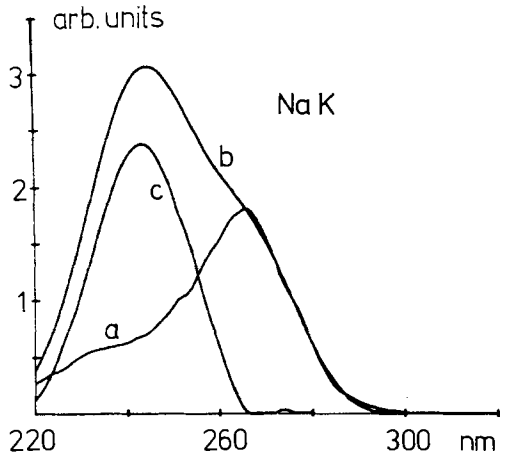

Fig. 20. *PIE. curves for NaK.* a) measured, b) calculated, and c) difference between b) and a)

Another channel, $NaK^* \rightarrow Na^- + K^+$, has an adiabatic threshold of 4.42 eV [1] and lowers the NaK^+ ion current detected. Both processes should augment the K^+ ion signal above the reconstructed curve. The experimental K^+ signal is indeed higher than the calculated curve. A contribution from the $K_2^* \rightarrow K + K^+ + e^-$ fragmentation process (4.85 eV) may, however, also be important. The different processes are difficult to disentangle with one-step photoionization experiments; 2-step laser photoionization measurements and lock-in techniques will soon provide a definite answer.

4. Two-photon-ionization (TPI.) spectroscopy. – The basic nature of the 2-photon absorption process (above) will now be discussed for the specific example of alkali dimer molecules. The first absorption step *(Fig. 21)* leads from the ground state $^1\Sigma_g^+$ to an excited state ($A^1\Sigma_u^+$, $B^1\Pi_u$, *etc.*). This *excitation* step at frequency ν_1 can be completely state-specific. Resolution is limited basically only by the collimation ratio of the molecular beam (which leads to a slight transverse velocity spread and concomitant *Doppler* broadening) or by the natural line width. Both are of the order of 20 MHz. Resolution for the broad scans presented is laser-limited to about 0.5 $cm^{-1} \triangleq 15$ GHz.

The excited molecules reside in the excited state for an average period $\tau = A_{10}^{-1}$ (fluorescent lifetime). If during this time the molecule absorbs a second photon at wavelength ν_2 (with $\nu_1 + \nu_2 >$ IE.) it will be *ionized,* either by a direct transition to a molecular ion state ($^2\Sigma_g^+$) or through an auto-ionizing *Rydberg* state.

Of course, the molecule residing in the intermediate excited level may absorb a second ν_1 photon, thereby being excited to a high electronic state of g parity. In the case of the Na_2 $^1\Sigma_u$ and the K_2 $^1\Pi_u$ states $\nu_1 <$ IE./2, so that molecules excited by double photon ($\nu_1 + \nu_1$) absorption are only detectable if ionized by a third photon. Although the probability for this process is extremely small at the low powers used, signals from ions generated by 3-photon absorption have been detected (see section 4.3).

If states with $\nu_1 >$ IE./2 are excited, ions may also be produced by absorption of 2 ν_1 photons. *Feldman et al.* [60] used this effect for the spectroscopic investigation of the Na_2 B←X system and for the $Ba + Cl_2$ reaction product BaCl. It can be completely eliminated by phase sensitive detection when chopping the ionizing laser beam (section 2).

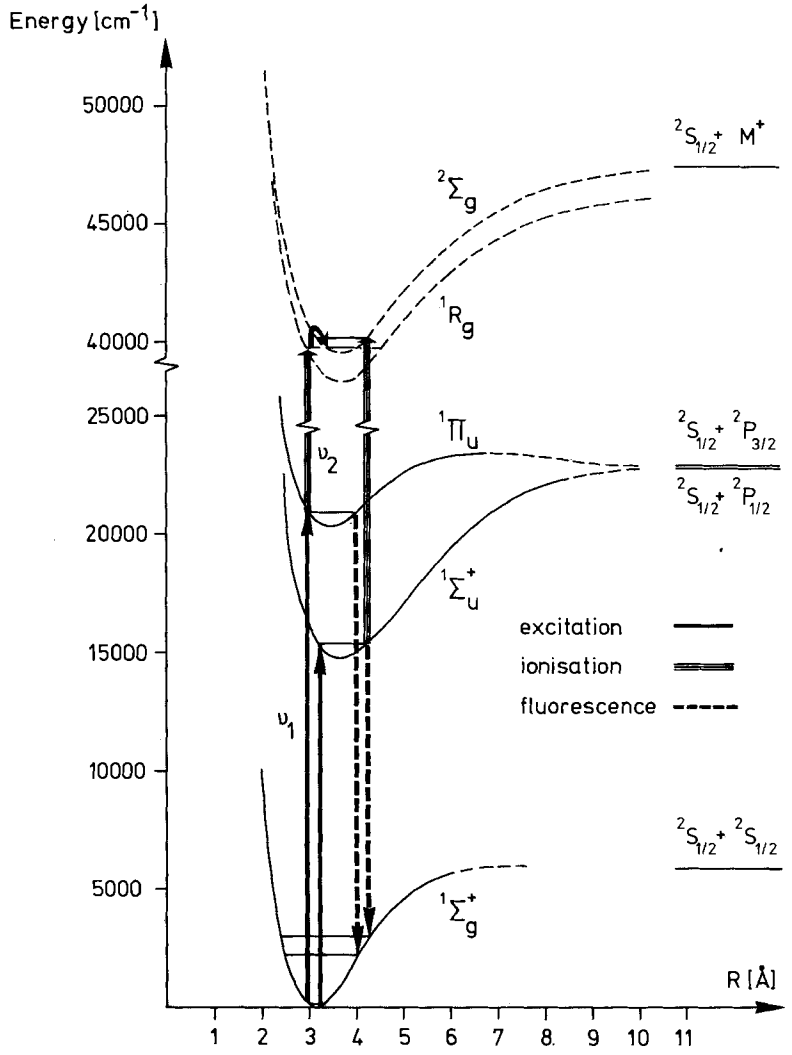

Fig. 21. *Potential energy curves for M_2 alkali dimers.* The $^1\Sigma_g^+$, $^1\Sigma_u^+$ and $^1\Pi_u$ are RKR-potentials from experimental data [53] [62]; the $^2\Sigma_g$ is an *ab initio* calculation [63], while the ^1R_g is a purely fictive *Rydberg* state

4.1. *Power dependences; optical pumping.* Before looking at the results of TPI. spectroscopy, it is necessary to summarize the possible excitation and deexcitation paths an alkali dimer can follow within the excitation scheme shown in *Figure 21*. A kinetic scheme is presented in *Figure 22*. A molecule is excited by stimulated absorption at rate $\sigma_{01} \cdot I_1$ (absorption cross section times photon flux). The excited molecule may do one of the following: 1) return to the ground state by stimulated emission (rate: $\sigma_{10} \cdot I_1$); 2) return to a different ground state level by fluorescence

(rate: A_{10}); 3) be ionized or excited to an autoionizing *Rydberg* state (rate: $\sigma_{12} \cdot I_2$); 4) be excited to a high-lying level indicated by ^1Z_g (rate: $\sigma_{13} \cdot I_1$).

The scheme is slightly simplified by making the following assumptions: 1) a dimer if excited to $^1\Sigma_u^+$ or ^1Z_g will not fluoresce back to exactly the same rovibronic state it started from. This process is sufficiently improbable to be neglected. 2) Radiative and collisional relaxation processes within the $^1\Sigma_g^+$ manifold are negligible. This is true for molecular-beam conditions and in the case of homonuclear diatomic molecules.

The differential equations describing the kinetics together with general and special solutions are presented in the *Appendix*. We are interested in the special solution obtained for weak-exciting photon fluxes (low I_1).

$$N_2 = N_0(0) \frac{\sigma_{12} \cdot I_2 \{1 - \exp(-\sigma_{01} I_1 t)\}}{(K\sigma_{01} + \sigma_{13}) I_1 + \sigma_{12} I_2 + A'_{10}} \tag{4}$$

N_2: ion flux [number of ions/(cm^2 · s)]
$N_0(0)$: dimer flux entering the ionization volume [molecules cm^{-2} s^{-1}]
t: time needed for a molecule to cross through the ionization volume ('residence time')

The dependence of the ion signal on I_1 (photon flux of the exciting laser) is of the form:

$$N_2 = \frac{A}{BI_1 + C} \{1 - \exp(-\sigma_{01} I_1 t)\} \tag{5}$$

For $BI_1 \ll C$ (the assumption with which (4) was derived) equation (5) simplifies to:

$$N_2 = A' \{1 - \exp(-\sigma_{01} I_1 t)\} \tag{6}$$

This simple dependence has been found for the low laser powers used for excitation *(Fig. 23a)*. In addition, we can derive a value for the absorption cross-section σ_{01}:

for $$\{1 - \exp(-\sigma_{01} I_1 t)\} = 0.5 \tag{7}$$

$$\sigma_{01} = \frac{\ln 2}{I_1 t} \qquad \text{is obtained.} \tag{8}$$

For 200 mW laser power at 6500 Å $I_1 = 1.3 \cdot 10^{20}\, h\nu/(\text{cm}^2 \cdot \text{s})$. The interaction time t is about 250 ns at a molecular velocity of 1000 m/s [45].

Thus $\sigma_{01} = \mathbf{2.1 \cdot 10^{-14}\ cm^2}$; the excitation rate $\sigma_{01} I_1$ at 200 mW is $2.7 \cdot 10^6$ s^{-1}.

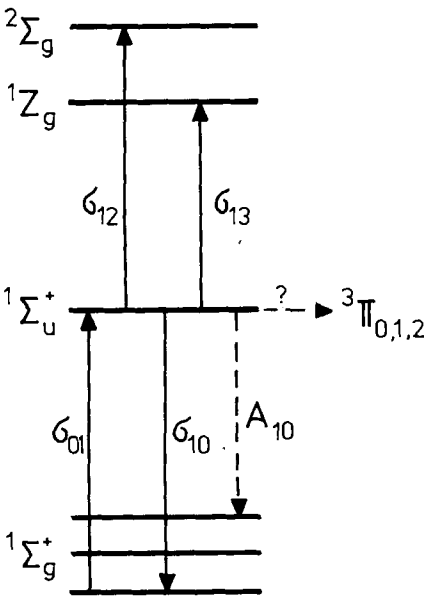

Fig. 22.
Simplified kinetic scheme for the TPI. process

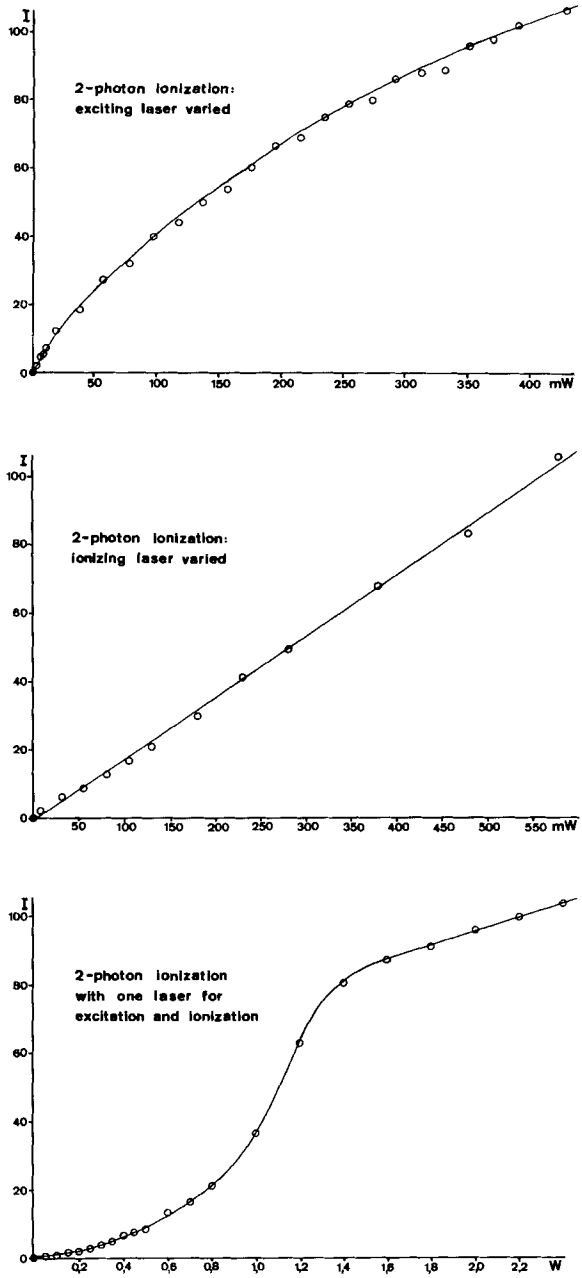

Fig. 23.
Dependence of ion signal on laser power for various spectroscopic arrangements

Fluorescence lifetimes in the Na_2 A–X band system are around 12 ns [46], so we are indeed justified in assuming that $BI_1 \ll C$ and $Z \gg Y$ (see *Appendix*).

The ion signal dependence on I_2 (photon flux of the ionizing laser) is of the form

$$N_2 = \frac{AI_2}{BI_2 + C} \tag{9}$$

Assuming that $BI_2 \ll C$, we find

$$N_2 = A' I_2 \tag{10}$$

This linear dependence has indeed be found *(Fig. 23b)* up to laser powers of 2 Watts. Evidently at very high powers (in the kW to MW range) N_2 will tend to the maximum value A/B. The ionization cross-section σ_{12} cannot be determined from the power dependence or other data given up to now. A separate experiment was made to determine the relative ionization probability in the following way.

The total beam flux at a constant oven temperature was measured at the *Langmuir-Taylor* detector, no radiation being incident on the beam. Then the Rhodamine B laser (400 mW at 6421 Å, corresponding to the Na_2 A–X; 9←0 transition) and the argon-ion laser (1.6 W UV. radiation at 350–365 nm) were focused into the beam in the usual way (see section 2). The decrease in signal at the *LT.* detector was now measured with a lock-in amplifier, the ionizing radiation being chopped. This decrease amounts to the rate at which Na_2 molecules are eliminated from the beam by 2-photon ionization, *i.e.* the ion flux N_2 of eq. (4). From the total beam flux and the dimer concentration in the beam the total dimer flux $N_0(0)$ can be calculated. The total probability for 2-photon ionization was thus found to be $\mathbf{p = N_2/N_0(0) = 2.5 \cdot 10^{-3}}$.

Estimating $\sigma_{13} \simeq \sigma_{01}$ and approximating $\kappa = 1$ (a very good approximation for high J) we can calculate σ_{12} from eq. (4). With $\sigma_{01} = 2.1 \cdot 10^{-14}$ cm^2 and $A_{10} = 10^8$ s^{-1} the photoionization cross-section turns out to be $\boldsymbol{\sigma_{12} = 6.5 \cdot 10^{-16}\ cm^2}$.

The cross-sections calculated above are dependent on the overlap of the spectral density of the lasers with the absorption line width of the molecular transitions. For the case of the exciting laser we may assume that the laser is spectrally homogeneous with a FWHM band width of $\Delta\tilde{\nu} = 0.5$ cm$^{-1} \triangleq 15$ GHz. At the band edge of a Na_2 A–X transition 6–7 P/R lines lie within this band width. The absorption line widths are about 15 MHz. Dividing the sum of the absorption line widths by the excitation band width we find a spectral overlap of 0.55%.

In the case of the ionizing laser we are exciting to a continuum of ionization energies, so the full laser band width is utilized. Should coincidences with an auto-ionizing transition occur, the cross-section may rise by a factor of $10^2 - 10^3$.

We are now able to interpret eq. (4) and our kinetic scheme *(Fig. 22)*. Molecules are pumped from the ground state to the intermediate excited state with a medium rate constant ($2.7 \cdot 10^6$ s^{-1}). If the radiation field is large enough, a specific ground state becomes depleted (optical pumping) [45] [47]. This effect is responsible for the $\{1 - \exp(-\sigma_{01} I_1 t)\}$ part of eq. (4), a functional dependence already found by *Visser et al.* [48], who measured the power dependence of dimer fluorescence.

An excited molecule may now return to a different ground state by fluorescing, a fast process (rate $\approx 10^8$ s^{-1}). Stimulated emission and absorption to higher non-ionizing states further diminish the excited state population (rate $\approx 2 \cdot 10^6$ s^{-1}). Normally the ionizing step has the smallest rate constant ($6.3 \cdot 10^5$ s^{-1} at 2 W laser power).

4.2. *TPI. spectroscopy: results.* – 4.2.1. *Isotope shifts for K_2.* The K_2 $B \leftarrow X$ absorption spectrum in the red spectral region (6700–6000 Å) is comfortably covered by the spectral range of a Rhodamine B dye laser. The K_2 molecules in the beam are present at their natural isotopic abundance ratios, *i.e.* $^{39,39}K_2/^{39,41}K_2/^{41,41}K_2$ 100:14.78:0.55. Using a sufficiently high resolution of the quadrupole mass-spectrometer, we have observed the spectral region for $m/e = 78$ and m/e 80 separately and were thereby able to measure the isotope shifts.

Table 3. *Isotope shifts for the $^{39}K_2$ and $^{39}K^{41}K$ molecules $B^1\Pi \leftarrow X^1\Sigma^+$*

Vibronic	Isotope shift		Difference
	measured	calculated	
Transition	[cm^{-1}]	[cm^{-1}]	[cm^{-1}]
0←1	−0.75	−1.224	0.47
0←0	1.00	0.102	0.90
1←0	1.51	0.799	0.71
2←0	3.01	1.683	1.33
3←0	3.26	2.551	0.71
4←0	4.02	3.403	0.61
5←0	6.28	4.240	2.04
6←0	5.52	5.065	0.46
7←0	6.78	5.877	0.90
8←0	7.78	6.677	1.10
9←0	8.79	7.446	1.32

The total values were calculated using atomic masses [49] and the appropriate molecular data [50]. The average of the differences between measured and calculated isotope shifts is 0.96 ± 0.47 cm^{-1} ($\pm$ one std. deviation). This systematic difference and the scatter indicate the accuracy and precision attainable with our present experimental configuration. These K_2 spectra were taken using NaK as feed to the molecular beam oven. The beam contained the particles Na, K, Na_2, NaK, K_2, Na_2K, NaK_2, K_3 and considerable concentrations of higher clusters, not counting the possible isotope combinations, yet the use of a mass-sensitive detection device allows complete separation of the highly overlapping absorption spectra.

4.2.2. *Intensity perturbations.* In TPI. spectroscopy the determination of true cross-sections σ_{01} is more complicated than usual, since the measured ion signal $N_2(v_1)$ is a function of several parameters (eq. (4)). The approximation that all parameters except σ_{01} are constant or slowly varying functions of v_1 is generally correct, but examples where this assumption is invalid have been found experimentally.

The 2 vibronic sequences of the K_2 $B^1\Pi_u \leftarrow X^1\Sigma_g^+$ system shown in *Figure 24* were taken using the same excitation source (Rh B laser, 140 mW, 0.5 cm^{-1} re-

solution); in the upper trace, ionization was performed with an Ar^+-ion laser (all lines, 20 W) and in the lower with the focused light of a 1 kW Hg lamp ($\lambda > 380$ nm). Comparison of the spectra shows strong intensity perturbations for the vibronic bandheads ($6 \leftarrow 0$) and ($6 \leftarrow 1$), reflecting variations in σ_{12}. The frequency continuum of the light provided by the high pressure lamp effectively smoothes out any frequency dependence. In the case of the Ar^+-ion laser the ionizing light is distributed into several very narrow lines ($\Delta\nu \simeq 0.3$ cm^{-1}), so that frequency variations of σ_{12} will be projected directly onto the spectra. Especially when the sum frequency $\nu_1 + \nu_2$ for any of the laser lines coincides with an autoionizing transition (see 4.3), σ_{12} may increase by a factor 10^2–10^3.

Variations in the other parameters (σ_{13}, A_{10}) may also exert a strong influence on the intensity of the ion signal. For alkali dimers, A_{10} is known to stay remarkably constant over a wide spectral range for both the $A \leftarrow X$ and $B \leftarrow X$ transitions [59] [46] [52]. The dependence of N_2 on σ_{13} is small as long as A_{10} is the dominating term in the denominator of eq. (4). Assuming that $\sigma_{13} \simeq \sigma_{01}$, it is evident that at least for low laser power I_1 even strong fluctuations in σ_{13} will not influence the ion signal significantly.

4.2.3. *Rotational structure and 'temperature'. Sinha et al.* [34] showed that alkali dimers undergo appreciable cooling during expansion in a supersonic nozzle beam. The vibrational temperature differed significantly from the rotational temperature owing to different relaxation rates with the vibrational and rotational modes. Our results show extensive cooling in both vibrational and rotational structure, the exact temperature being a sensitive function of the stagnation pressure p for a given nozzle of diameter d.

For the K_2 spectra in *Figure 24* the stagnation pressure was ~ 100 Torr and the nozzle diameter was 0.2 mm. Only $v' \leftarrow 0$ and $v' \leftarrow 1$ bands are visible in the spectra and we calculate a vibrational temperature of $45 \pm 10°$ K (the standard-deviation is due to the overlapping of the $v' \leftarrow 0$ and $v' \leftarrow 1$ bands, which leads to increased uncertainties in the intensity measurements). We also measured the rotational temperature of Na_2 at several stagnation pressures and find a roughly inverse relationship *(Fig. 25)*. Two rovibronic scans covering the vibronic transition $9 \leftarrow 0$ from the bandhead to the $8 \leftarrow 0$ bandhead are shown in *Figure 25*. At low stagnation pressure (approximately 15 Torr) the rotational temperature is $90 \pm 10°$ K *(Fig. 25a)*. Increasing the stagnation pressure by a factor of 7 produces a rotationally much colder beam: $T_{rot} = 25 \pm 5°$ K. The rotational temperatures were determined by calculating the rovibronic line frequencies [53] and intensities, assuming a *Boltzmann* ground state distribution. The lines were convoluted with a gaussian line shape of 0.5 cm^{-1} FWHM line width. By varying the temperature as parameter, a least-square fit to the experimental data was performed.

4.3. *Photoionization spectra.* If one uses a second tunable dye laser as a source of ionizing radiation it is possible to measure the ion signal as a function of the ionizing frequency ν_2 and thus obtain information on PI. thresholds, autoionizing molecular *Rydberg* states and molecular ion states.

The K_2 molecule is an obvious candidate for this type of experiment because of its low PI. threshold (see *Table 1*). For the excitation step a low-power (200 mW) Rhodamine B cw dye laser was tuned to successive vibronic band heads of the K_2 $^1\Pi_u \leftarrow {}^1\Sigma_g^+$ (B-X) band system over a wavelength range from 6507–6167 Å, cor-

responding to the $0\leftarrow 0$ to $12\leftarrow 0$ ($v'\leftarrow v''$) transitions. At a resolution of 2.0 ± 0.2 cm^{-1} FWHM between 45 and 60 different P, Q, R transitions near the band edge are excited. For the ionization step a Rhodamine 6G cw dye laser was tuned from 6030 to 5760 Å. Excitation of high v'; $^1\Pi_u$ levels in this wavelength region is

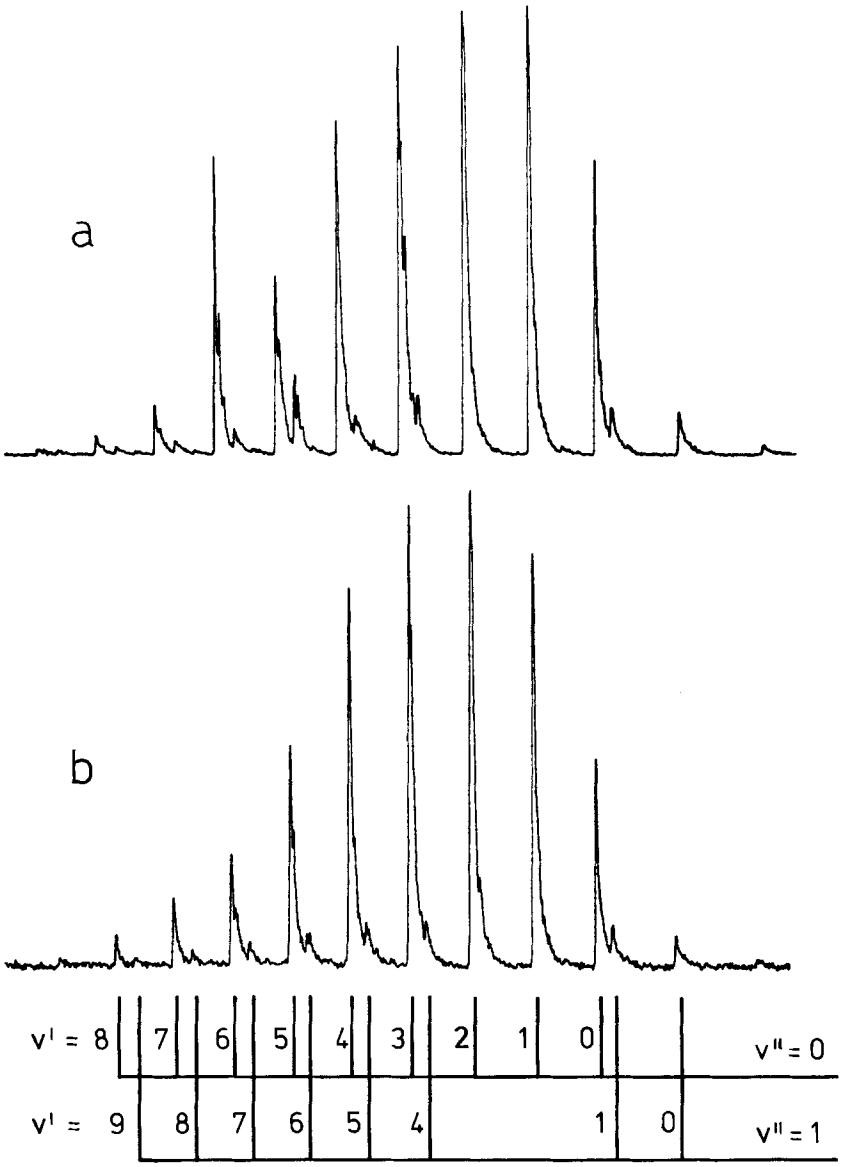

Fig. 24. *Vibronic TPI. spectra of the* $K_2\ B^1\Pi_u \leftarrow X^1\Sigma_g$ *band*
a) ionization with a discrete line source (Ar^+-laser); note autoionization perturbations (at $6\leftarrow 1$) and ($6\leftarrow 0$)).
b) ionization with a continuum source (1 kW Hg Lamp)

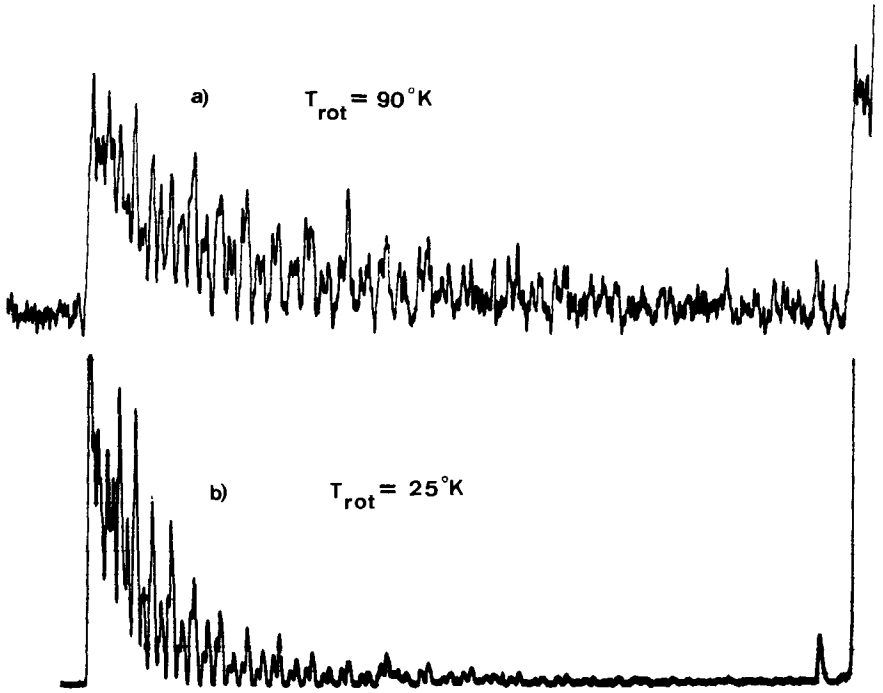

Fig. 25. *Rovibronic scans of the* $Na_2\, A\,^1\Sigma_u^+ \leftarrow X\,^1\Sigma_g^+ (9' \leftarrow 0'')$ *band*
a) rotational temperature 90° K with 15 Torr pressure in the oven cartridge. The small beam intensity causes noticeable signal fluctuations
b) rotational temperature 25° K with 105 Torr pressure.
The *Boltzmann* distribution has been fitted to the intensities of the P/R-progressions, modified in the J″ = even/J″ = odd intensities by nuclear spin of 3/2 to 3/5

extremely improbable, *Franck-Condon* factors for these transitions being below 10^{-3}. Recording the K_2^+ photoion signal as function of v_2 at fixed v_1 provides high-resolution PI. efficiency curves, 2 of which are presented on *Figure 26.*

Contrary to the low-resolution one-step PI. curves shown in section 3 these high-resolution curves are characterized by strong autoionization features superimposed on a comparatively weak continuum. The ratio of the highest autoionization peaks to the continuum reaches 10^2–10^3. This explains the distortion of TPI. spectra pointed out in 4.1. When ionizing with the narrow band width lines of an Ar-ion or a Kr-ion laser, chance coincidences with autoionizing peaks will intensify the ion signal at certain *excitation* frequencies. On the other hand, the inherently low efficiency of the ionization step may be increased by choosing a favourable wavelength.

PIE. curves *via* different intermediate vibronic levels of the $^1\Pi_u$ state show progressive changes in autoionization structure going from low intermediate v′ to high v′ but differ pronouncedly when comparing curves *via* extremely high and low vibronic levels, as in *Figure 26.* The continuum-to-background ratio decreases with increasing v_2, reflecting a decrease in *Franck-Condon* factors for direct ionization.

No step structure in the photoionization continuum is discernible so that spectroscopic information on the K_2^+ molecular ion cannot be obtained directly with this method. This situation is not specific to the K_2^+ PIE. curves, but is found for all homonuclear diatomic molecules [54] [55]. On the other hand, higher vibrational levels of the K_2^+ $^2\Sigma_g^+$ ground state as well as the higher electronic ion

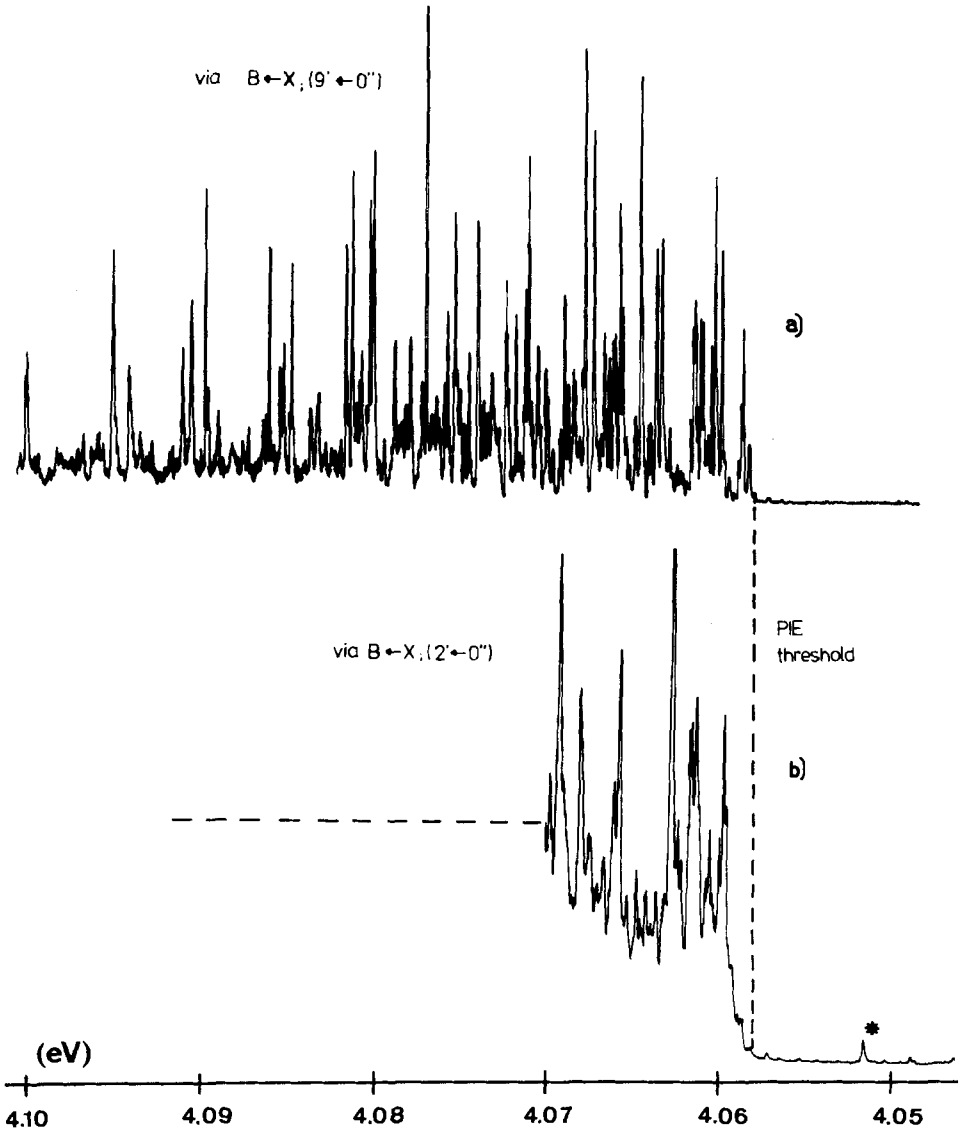

Fig. 26. *Two-step laser PIE. curves for K_2 with different v' for the intermediate $B^1\Pi_u$-state.* The very complicated spectra span an energy region of 0.05 eV and are completely reproducible in every small detail. The upper curve with v'=9 shows a large number of superimposed autoionization progressions and almost no continuum due to direct ionization contrary to the lower curve with v'=2, where less specific effects but a large (dashed line) general ion current can be observed. The small peak with an asterisk in the pre-threshold region is a 3-PI. transition.

states ($^2\Pi_u$, $^2\Sigma_g(3p)$) should be identifiable as convergence limits of the appropriate *Rydberg* progressions in the PIE. curves. Such progressions have been tentatively identified in the case of very intense autoionization peaks, but assignment of medium and weak progressions is difficult owing to the enormously complicated structure.

PI. thresholds for K_2 measured by one-step and 2-step PI. methods are summarized in *Table 4*. The last value, although representing the most accurate value of the K_2 PI. threshold to date, is still not quite free of doubt: PI. thresholds *via* successive $^1\Pi_u;v'$ states show no distinctive trend but scatter more or less randomly around the mean value with a standard deviation significantly greater than the experimental accuracy (*cf.* values 3, 4 and 5 of *Table 4*).

This difference is attributed to several problems.

a) For low intermediate v' *(Fig. 26b)* the PI. threshold is clearly defined by the onset step of direct ionization. For high intermediate v' only an upper boundary to the threshold can be given by noting the appearance of definite autoionization structure.

b) The pre-threshold region is not completely devoid of ion signal, but shows low-intensity peaks reproducible in position and intensity. The laser power dependence of the strongest signal in *Figure 26b* (marked with an asterisk) has been measured and found to be linear in $P(\nu_1)$ (with the usual optical pumping effect) and quadratic in $P(\nu_2)$ indicating *3-photon ionization*. Signals of this type lying closely below the PI. threshold are difficult to distinguish from weak autoionization structure at threshold and thereby jeopardize an unambiguous determination of the threshold value.

c) *Rydberg* states lying slightly beyond the ionization threshold may be ionized by additional electric fields present in the ionization region. The fields necessary to ionize high-lying *Rydberg* states can be quite weak. A dramatic example of this phenomenon was pointed out by *Chupka & Berkowitz* [54] in the H_2 molecule: the R(1) line of the B''–X (4,0) transition is absent at 600 V/m but ionizes at $2.2 \cdot 10^3$ V/m. Field ionization as a high-efficiency detection technique for *Rydberg* states of atomic Na was used by *Ducas et al.* [56]. The main perturbing fields in our case are due to the voltage on the repeller electrode and to the oscillating electric fields of the laser beams. Repeller voltages varied from 10 to 40 V in our experiments, equivalent to fields of $0.5\text{–}2 \cdot 10^3$ V/m.

The peak electric field amplitude E^0 of a light wave may be calculated from the root-mean-square irradiance J_{rms}. The electric field of a 2.0 W laser beam focused to 0.5 mm^2 ($J_{rms} = 4 \cdot 10^6$ W m^{-2}), is

$$E^0 = \sqrt{2Z^0 J_{rms}} = \mathbf{5.5 \cdot 10^4\ V/m}$$

Z^0: impedance of free space = 377Ω.

An intuitive basis for comparison may be provided by the following order of magnitude calculation: for a *Rydberg* orbital with high n we replace the molecular core by the corresponding united atom, in our case Sr with the ground state configuration [Kr] $5s^2$. Using *Slater* shielding parameters, we calculate a $Z_{eff} = 3.7$ felt by a 5*s* electron. For a circular *Bohr* orbit with principal quantum number n = 25 the orbit radius is $r = (a_0/Z_{eff}) \cdot n^2 = 8.95$ nm. At this distance the electric field due to the core is $6.65 \cdot 10^7$ V/m, *i.e.* the perturbing fields of the laser and the repeller are roughly 10^{-3} and $2 \cdot 10^{-5}$ of the *Coulomb* field experienced by the *Rydberg* electron.

These perturbations are modest but measurable: for the orbit radius and light intensity given above we find a potential drop of almost 1 mV across the *Rydberg* atomic diameter, which in spectroscopic terms corresponds to an energy of 8 cm^{-1}.

Table 4. *PI. thresholds for K_2*

Method	Energy [eV]	Ref.
1-step PI.	4.0 ±0.1	[27]
1-step PI.	4.05 ±0.05	[1]
2-step PI. (v' = 2)	4.060 ± 0.0005	this work
2-step PI. (v' = 9)	4.061 ± 0.0005	this work
2-step PI. mean value (v' = 1–10)	4.059 ± 0.001	this work

5. Discussion. – 5.1. *Alkali-metal clusters* are easily formed in supersonic nozzle expansions [27] [37] [1]. Their size/abundance distribution can be varied within wide limits by changing the temperature/pressure in the oven and its orifice diameter [36]. One might hope to create paucidispersions of predetermined first and second moments by proper control of the collisional processes during vapour expansion. *Other metals* will behave similarly: group IIb has been partly investigated (*e.g.* $\leqslant Hg_8$). For most metals a high-temperature oven is necessary (now under construction). Transition metals, especially of the 5*d* series, cannot be clustered by the same technique. However, co-expansion with rare gases provides the necessary cooling even at small saturation pressures.

The *photoionization-potential* (PIP.) of the Na molecules $\leqslant Na_{14}$ is the longest contiguous series of any intrinsic cluster property known today. The pioneering measurements [27] [37] have been both less complete and precise. As pointed out [1], the general trend of the PIP. convincingly follows a curve determined by the excess work function due to the convex surface of small particles. A cluster may be idealized as a conducting sphere and compared to an infinite flat metallic surface. The potential energy for removing an elementary charge is larger for the sphere, because the image charge moves only from the surface to the centre while the real charge goes to infinity. In the flat slab the image charge is always as far behind the surface as the real charge is in front, *i.e.* both charges go to infinity. The difference amounts to $e^2/2R$ if R = radius of cluster sphere and reaches values of 1.5–3 eV below $M_{x\lesssim 10}$. Superimposed on this general trend are the proper quantum chemical effects of the ground state electron configurations as characteristic for a certain x and the pertinent molecular symmetry.

The most spectacular deviations from uniform behaviour are exhibited by the M_3 particles. The underlying *quantum chemistry* is well understood and has been extensively documented for Li_3 [3], where the results of PNO-CEPA-CI *ab initio* calculations and the full treatment of the dynamic *Jahn-Teller* effect together with the nuclear probability densities of many vibronic states are given. The total energy compared to the separated, stationary atoms (atomization energy at 0° K) is about 40 kcal/mol in good agreement with the experimental value of *Wu* [11]. The spin density of the odd electron in Li_3 is almost exactly the same as experimentally found by *Lindsay, Herschbach & Kwiram* [16] for Na_3 in an Ar-matrix.

If *high-symmetry 3-dimensional clusters* are assumed irrespective of the distortions by *Jahn-Teller* splittings of degenerate states, the first Na_x after Na_2 with a closed shell ground state configuration is cubic Na_8. The dip in the PIP. *(Fig. 13)* at x = 8 and a marked decrease in the Na_x-abundance curve after x = 8 are compatible with a preferred stability. No such indications can be given within the precision obtained for bcc-Na_9, Na_{12} (icosahedron), Na_{13} (bc-icosahedron) or Na_{14} (double bc-cube with common face).

The question of *isomers* in mixed molecules arises first with the trinuclear species where the series Na_3, Na_2K, NaK_2 and K_3 have been measured. The sharp threshold and the values 3.98, 3.7, 3.62, 3.3 eV in the same sequence are well represented by the interpolation formula (3). No indication of two thresholds for NaKNa, KNaNa or NaKK, KNaK have been observed. According to the semi-empirical model potential perturbation treatment of *Hart & Goodfriend* [57]

differences of 0.38 and 0.26 eV should exist between the two isomer pairs if they form linear molecules. *Gerber & Schumacher* have shown [3] that Li_3 has an obtuse isosceles triangular ground state. Its vibrational modes allow an exchange of atoms which, with Na_2K or NaK_2, is expected to happen at low temperature because the activation energy is only of the order $\lesssim 500$ cm^{-1}. This rationalizes the unobservability of isomers.

On average, Li_3 is in a *fluxional* D_{3h} *geometry* because the 3 minima on the *Born-Oppenheimer* hypersurface spanned by Q_x, Q_y (Q_x, Q_y are the normal coordinates which form a basis of the E′ irreducible representation) are connected by saddlepoints whose height is already exceeded by the zero point vibrational energy [3]. This is expected to be true for Na_3, K_3 and the heteronuclear triatomics. The behaviour is reflected in the soft, malleable nature of the macroscopic bulk metal and stereochemical effects of a rigid structure are not foreseen to be dominant in these clusters.

Figure 27 shows a part of the *TPI. spectrum of* Na_3 between 6900 and 5970 Å, whose completion is in progress. At a resolution of 0.5 cm^{-1} no rotational structure is recognizable. The bands found are tentatively assigned to the allowed electronic

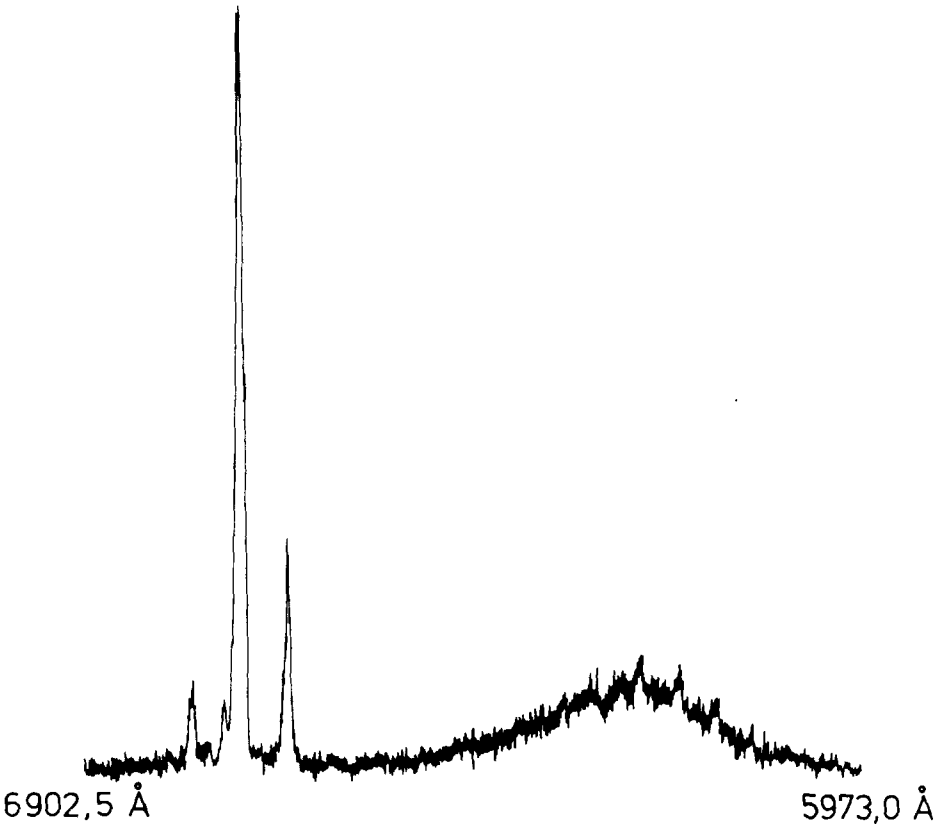

Fig. 27. *TPI. spectrum of* Na_3 *as recorded by a mass-spectrometer at* m/e = *69* (sensitivity of the two largest peaks × 0.5). The wavelength of the exciting laser beam has been tuned from 6902.5 to 5973 Å.

doublet-doublet transitions $1e'' \leftarrow 1e'$, $1e' \leftarrow 1a_1'$, $3a_1' \leftarrow 1e'$ (larger λ) (D_{3h} average) as suggested by SCF-Xα-SW calculations performed by *E. Scholl* in our laboratory. Spectral details of this gaseous molecule are much superior to those obtainable by matrix isolation spectroscopy shown for Ag_3 by *Schulze & Becker* [14]. In view of the soft deformation modes of these molecules and the remarkable matrix-guest interactions revealed by matrix-shifts, we have considerable doubts whether matrix spectra are able to yield intrinsic structural information on trimers.

The spectral range of the observed Na_3 sequence belongs to electronic transitions. There is no doubt, therefore, that Na_3 is a 'genuine' molecule with its unique electronic states and not merely a weak *Van der Waals* adduct of 3 Na or $Na_2 + Na$ as has been observed in cold supersonic beams of for example rare gas atoms, H_2, H_2O or CO_2 molecules [58]. We are thus able to confirm and to extend the conclusion drawn by *Lindsay et al.* [16] from the ESR. spectrum of Na_3. Since H_3 is not a stable molecule – the 3 shallow minima on the static *Jahn-Teller* surface do not accomodate the zero point vibrational energy [59] – this fact is interesting but not unexpected. The bonding features of H-atoms are unique and not exactly extendable to the behaviour of other monovalent atoms. There are no or very low stereoelectronic requirements for the bonding of atoms through *s*-states (in an LCAO-MO parlance); hence there is no hindrance for *Van der Waals* collision complexes of Na atoms to snap into an electronically bonded molecule, if the environment assists removal of the excess angular momentum by further collisions. Obviously, this mechanism is very effective in the supersonic expansion process as revealed by a 'temperature' $< 100°$ K for the internal degrees of freedom.

5.2. *Two- or multi-photon ionization spectroscopy* with mass-spectrometric detection is a tool of considerable potential for cluster-work and for many other applications, *e.g.* where spectral information on parent molecules or fragments might be of help to interprete MS. or to study otherwise unobservable molecular species. In special cases, using simple ion detection, *e.g.* a channeltron, it can lead to well resolved vibrational spectra, as shown independently for Na_2 and BaCl by *Feldman et al.* [60]. In a mixture with species of overlapping spectra, the mass-spectrometer serves to discriminate them. The narrow band width of laser radiation allows selection of specific gyrovibronic transitions at least in smaller molecules. In order to obtain large spectral scans, resolution has to be partially sacrificed for minimization of data acquisition time. It is always possible, however, to resolve a particular spectral window to ~ 10 MHz $= 0.0003$ cm^{-1}, ample for the observation of isotope effects and hyperfine interactions.

The present limits of the method are defined by several parameters:

– *spectral range:* tunable cw dye lasers now cover a wavelength range from 400–960 nm. This may seem a serious limitation since many molecular states of interest lie in the near UV. or further in the IR. By using nitrogen-laser pumped dye lasers these limits may be pushed further in both directions, but this has to be paid for by longer acquisition times (much lower duty cycle of pulsed lasers). In addition, great care has to be exercised in the interpretation of the spectra as higher order processes become much more important.

– *ionization energy:* the lowest wavelength available with sufficient flux for the ionization step depends on the type of experiment planned. For cw experiments,

high-pressure Hg lamps deliver strong fluxes down to ~240 nm. For pulsed experiments the powerful rare gas halide excimer lasers can be used (ArF 193 nm, KrF 248 nm). Adding the photon energies for the 2 steps shows that the method is at present limited to particles with an IE. below 9 eV.

Extension to higher IE. will be possible using a combination of photon excitation and electron impact or field ionization, multi-photon processes [60] or synchrotron radiation.

– *sensitivity:* it is possible to raise the sensitivity at least by a factor of 100 above the current values by improving the experimental configuration (increased ionizing laser power by using the full intra-cavity power). The very high sensitivity of the TPI. method was recently demonstrated for atoms by *Hurst et al.* [61]. The sensitivity is somewhat smaller for molecules, as they are distributed over 10^3 microstates, depending on temperature and moments of inertia of the molecule. Only a small part of these states are excited, depending on the laser band width. Since (for the limit of high ionization laser power) every excited molecule can be ionized, and practically all ions produced can be collected and measured, TPI. is by far the most sensitive method for the measurement of molecular absorption spectra.

This research has been supported by the *Swiss National Science Foundation*, grants 2.034.73, 2.475-0.75, 2.660-0.76, for which we are very grateful.

H. Labhart†, Zürich, helped our start in spring 1974 by stimulating discussions and by loan of 2 CH-4 mass spectrometers. *R. N. Zare*, Stanford, and *H. Weber*, Bern, have generously supplied advice. We further thank *H. Pauly*, Göttingen, for instructive discussions on molecular beam apparatus, *U. Wild* (ETH-Z), *P. Anliker* (Bern), and *W. Heinzelmann* (Univ.Z.) for lending equipment. *U. Bill*, and *M. Gygax* helped with the design of the apparatus and realized its construction and *K. Schindler* supplied part of the electronics. *U. Grünwald* made the engineering drawings.

Appendix. – The kinetic analysis of the experimental situation presented in TPI. experiments is based on the simplified energy-level diagram shown in *Figure 22*.

The energy level diagram is not complete inasmuch as no explicit mention is made of triplet levels, which may play a decisive role in changing the whole kinetics of the system. We will disregard the problem: first, no exact information is yet obtainable on intersystem-crossing and triplet luminescence rates; secondly, the influence of the triplet states on the ion flux may be mathematically incorporated in form of an 'effective' fluorescence lifetime A'_{10}.

Let the population in $^1\Sigma_g^+$, $^1\Sigma_u$, $^2\Sigma_g$ be denoted by N_0, N_1, N_2. The cross-sections and rate constants have been explained in section 4.1. The cross-sections for stimulated absorption and emission σ_{01} and σ_{10} are related in the same way as the *Einstein B* coefficients:

$$\sigma_{10} = \kappa\sigma_{01} = \frac{g_0}{g_1}\sigma_{01} = \frac{(2J''+1)}{(2J'+1)}\sigma_{01} \tag{11}$$

The rate equation for $N_1(t)$ is:

$$\frac{dN_1}{dt} = N_0\sigma_{01}I_1 - \{(\kappa\sigma_{01}+\sigma_{13})I_1 + \sigma_{12}I_2 + A'_{10}\}N_1 \tag{12}$$

For the boundary conditions:

$$N_1(t=0)=0 \qquad N_0(t=0)=N_0(0)$$

and setting:

$$Y = \sigma_{01} I_1$$

$$Z = \{(\kappa\sigma_{01} + \sigma_{13}) I_1 + \sigma_{12} I_2 + A'_{10}\}$$

we obtain the solution:

$$\mathbf{N_1(t) = N_0(0) \frac{Y}{Z-Y} (e^{-Yt} - e^{-Zt})} \tag{13}$$

The rate equation for N_2 is:

$$\frac{dN_2}{dt} = N_1 \sigma_{12} I_2 \tag{14}$$

$$N_2(t) = \sigma_{12} I_2 \int_0^t N_1 \, dt; \quad \text{with eq. (13)}$$

$$\mathbf{N_2(t) = \frac{N_0(0) \sigma_{12} I_2 \cdot Y}{Z-Y} \{\frac{1}{Y}(1 - e^{-Yt}) - \frac{1}{Z}(1 - e^{-Zt})\}} \tag{15}$$

In our case the upper integration limit t is the residence time in the interaction volume. The residence time is defined by the length of the interaction zone Δx and the molecular velocity v by $t = \Delta x/v$. Eq. (15) is therefore only applicable to a class of molecules with the same velocity. In a supersonic beam, however, the velocity distribution is quite sharply peaked [33] [45], so we can assume an average velocity without introducing a large error. For effusive beams or for more exact calculations eq. (15) has to be convoluted with the velocity distribution N(v). Three limiting cases of the general equation (15) will now be discussed in more detail:

1) for $Z \gg Y$:

$$N_2(t) = \frac{N_0(0) \sigma_{12} I_2}{(\kappa\sigma_{01} + \sigma_{13}) I_1 + \sigma_{12} I_2 + A'_{10}} (1 - e^{-\sigma_{01} I_1 t}) \tag{16}$$

This limiting case is realistic for small excitation intensities I_1 and therefore appropriate to the experimental conditions described in section 4.

2) for $Y \gg Z$: it follows that $\sigma_{01} I_1 \gg \kappa\sigma_{01} I_1$ which is physically impossible. For dimer molecules $1/3 \leqslant \kappa \leqslant 3$ using the selection rule $\Delta J = 0, \pm 1$.

3) for $Y \simeq Z$:

Stimulated absorption and emission are very fast compared to all other rates, *i.e.* the transition is optically saturated. In this case the approximation on which the calculation is based breaks down, *i.e.* we can no longer use first order time-dependent perturbation theory as a basis for calculation of transition rates.

REFERENCES

[1] *A. Herrmann, E. Schumacher & L. Wöste:* Preparation and Photoionization Potentials of Molecules of Sodium, Potassium and Mixed Atoms, J. chem. Physics, in print.

[2] *A. Herrmann, S. Leutwyler, E. Schumacher & L. Wöste:* Multiphoton Ionization: Mass Selective Laser-Spectroscopy of Na_2 and K_2 in Molecular Beams, Chem. Physics Letters *52*, 418 (1977).

[3] *W. H. Gerber & E. Schumacher:* The Dynamic *Jahn-Teller* Effect in the Electronic Groundstate of Li_3, J. Chem. Physics, submitted 28.10.1977.

[4] *E.g. R. A. Potts, R. D. Barnes & J. D. Corbett,* Inorg. Chemistry *7*, 2558 (1968), and ref. cited therein.

[5] *M. J. Taylor,* 'Metal-to-Metal Bonded States of the Main Group Elements', Academic Press, London 1975; *L. Malatesta & S. Cenini,* 'Zerovalent Compounds of Metals', Academic Press, London 1974.
[6] Term defined by *J. A. Betrand, F. A. Cotton & W. A. Dollase,* Inorg. Chemistry *2*, 1166 (1963).
[7] Triple bonded W≡W: *M. H. Chisholm, F.A. Cotton, M. W. Extine, M. Millar & B. R. Stults,* Inorg. Chemistry *16*, 320, 603 (1977); furthermore quadruply bonded W≡W: *D. M. Collins, F. A. Cotton, S. Koch, M. Millar & C. A. Musillo,* J. Amer. chem. Soc. *99*, 1259 (1977).
[8] *M. Mc.Partlin, R. Mason & L. Malatesta,* Chem. Commun. *1969*, 334.
[9] *L. V. Interrante et al.,* Inorg. Chemistry *10*, 1169, 1174 (1971).
[10] *E.g. J. A. Rabo,* 'Zeolite Chemistry and Catalysis', ACS Monograph 171 (1976), chapter 10.
[11] *C. H. Wu,* J. chem. Physics *65*, 3181 (1976).
[12] See lit. in [1].
[13] *E.g. E. P. Kündig, M. Moskowits & G. A. Ozin,* Angew. Chem. *87*, 314 (1975); *A. G. Gaydon,* 'Dissociation Energies and Spectra of Diatomic Molecules', 3rd ed., Chapman & Hall, London 1968.
[14] *W. Schulze, H. U. Becker & D. Leutloff,* J. de Phys. *C2*, 7 (1977); *W. Schulze, H. U. Becker & H. Abe,* Intern. Conf. on Matrix Isolation Spectroscopy, June 21–24, 1977, Berlin West; Matrix Raman Spectra of Ag_2 and Ag_3, *W. Schulze & H. U. Becker,* to be published.
[15] *M. Moskowits & J. E. Hulse,* J. chem. Physics *66*, 3988 (1977).
[16] *D. M. Lindsay, D. R. Herschbach & A. L. Kwiram,* Mol. Physics *32*, 1199 (1976).
[17] Intense colours and other spectroscopic observations of Na_x and other molecules in zeolites will be described in a forthcoming paper by A. Herrmann & E. S. Schumacher.
[18] *E.g. S. Leutwyler & E. Schumacher,* Chimia *31*, 475 (1977).
[19] *C. Solliard & Ph. Buffat,* J. de Phys. *C2*, 167 (1977); *Ph. Buffat & J.-P. Borel,* Phys. Rev. A *13*, 2287 (1976).
[20] *J. Farges;* similarly *R. Jeuck & G. D. Stein,* Intern. Meeting on Small Particles, Lyon 1976.
[21] *B. G. Bagley,* Nature *225*, 1040 (1970); *M. R. Hoare & P. Pal,* J. Crystal Growth *17*, 77 (1972); *J. J. Burton,* Cat. Rev. Sci. Eng. *9*, 209 (1974).
[22] *A. L. Robinson,* Science *185*, 772 (1975).
[23] *H. P. Härri & E. Schumacher* have found product yield differences in dehalogenation reactions of $C_2H_2Cl_2$ and $C_2H_2Br_2$ by Na (bulk) against Na (clusters); diploma thesis of H. P. Härri, Bern 1977.
[24] Compare *K. H. Johnson,* Chimia *31*, 411 (1977).
[25] *P. L. Timms,* Adv. in inorg. Chemistry and Radiochemistry *14*, 121 (1972); Angew. Chem. *87*, 295 (1975).
[26] *L. Brewer, B. A. King, J. L. Wang, B. Meyer & G. F. Moore,* J. chem. Physics *49*, 5209 (1968); *L. Brewer & C. Chang,* J. chem. Physics *56*, 1728 (1972); see *B. Meyer,* 'Low Temperature spectroscopy', Elsevier, N.Y. 1971.
[27] *E. J. Robbins, R. E. Leckenby & P. Willis,* Adv. Physics *16*, 739 (1967).
[28] *H. U. Lee & R. N. Zare,* J. chem. Physics *64*, 431 (1976).
[29] *R. Tschudin & E. Schumacher,* unpublished; *R. Tschudin,* diploma thesis, Bern 1976.
[30] *E. Schumacher & R. Taubenest,* Helv. *47*, 1525 (1964); ibid. *49*, 1447 (1966) (Ni_2, Mo_2, Fe_2).
[31] *K. Kimoto & I. Nishida,* J. phys. Soc. Japan *42*, 2071 (1977).
[32] *M. G. Mason & R. C. Baetzold,* J. chem. Physics *64*, 271 (1976).
[33] *R. J. Gordon, Y. T. Lee & D. R. Herschbach,* J. chem. Physics *54*, 2394 (1971).
[34] *M. P. Sinha, A. Schulz & R. N. Zare,* J. chem. Physics *58*, 549 (1973).
[35] *R. Schieder, H. Walther & L. Wöste,* Opt. Commun. *5*, 337 (1972).
[36] *A. Herrmann, S. Leutwyler, E. Schumacher & L. Wöste,* to be published.
[37] *P. J. Foster, R. E. Leckenby & E. J. Robbins,* J. Physics *B2*, 478 (1969).
[38] *B. Wellegehausen, H. Welling & R. Beigang,* Appl. Physics *3*, 387 (1974).
[39] *S. Leutwyler, E. Schumacher & L. Wöste,* Opt. Commun. *19*, 197 (1976).
[40] *H. W. Kogelnik, E. P. Ippen, A. Dienes & C. V. Shank,* I.E.E.E. Quant. Electronics *8*, 373 (1972).
[41] *A. L. Bloom,* Appl. Optics (1975).
[42] *H. W. Schröder, H. Dux & H. Welling,* Appl. Physics (1975).
[43] *P. M. Guyon & J. Berkowitz,* J. chem. Physics *54*, 1814 (1971).
[44] *M. Leleyter & P. Joyes,* Radiation Effects *18*, 105 (1973).
[45] *K. Bergmann, U. Hefter & P. Hering,* J. chem. Physics *65*, 488 (1976).

[46] *T. W. Ducas, M. G. Littman, M. L. Zimmerman & D. Kleppner,* J. chem. Physics *65*, 842 (1976).
[47] *R. E. Drullinger & R. N. Zare,* J. chem. Physics *51*, 5532 (1969).
[48] *A. G. Visser, J. P. Bekooy, L. K. van der Meiz, D. de Vreugd & J. Korving,* J. chem. Physics *20*, 391 (1977).
[49] *H. Kienitz,* «Massenspektrometrie», Verlag Chemie, Weinheim 1968.
[50] *G. Herzberg,* 'Spectra of Diatomic Molecules', van Nostrand, New York 1950.
[51] *W. Demtröder, W. Stetzenbach, M. Stock & J. Witt,* J. mol. Spectroscopy *61*, 382 (1976).
[52] *P. H. Wine & L. A. Melton,* Chem. Physics Letters *45*, 509 (1977).
[53] The *Dunham* coefficients were taken from: *W. Demtröder & M. Stock*, J. molec. Spectrosc. *55*, 476 (1975) for the X state; *P. Kusch & M. M. Hessel,* J. chem. Physics *63*, 4087 (1975) for the A state.
[54] *W. A. Chupka & J. Berkowitz,* J. chem. Physics *51*, 4244 (1969).
[55] *P. M. Dehmer & W. A. Chupka,* J. chem. Physics *62*, 4525 (1975).
[56] *T. W. Ducas, M. G. Littman, R. R. Freeman & D. Kleppner,* Phys. Rev. Letters *35*, 366 (1975).
[57] *G. A. Hart & P. L. Goodfriend,* Mol. Physics *29*, 1109 (1975); J. chem. Physics *62*, 1306 (1975).
[58] *O. F. Hagena & W. Obert,* J. chem. Physics *56*, 1793 (1972); *A. van Deursen, A. van Lumig & J. Reuss,* Int. J. Mass Spectr. Ion Phys. *18*, 129 (1975); *R. P. Hemenger,* J. chem. Physics *66*, 1795 (1977).
[59] *R. N. Porter & M. Karplus,* J. chem. Physics *40*, 1105 (1964); *R. N. Porter, R. M. Stevens & M. Karplus,* ibid. *49*, 5163 (1968); *A. J. C. Varandas & J. N. Murrel,* Faraday Disc. No. *62*, 92 (1977), where the static H_3 *Jahn-Teller* problem is treated.
[60] *D. L. Feldman, R. K. Lengel & R. N. Zare,* Chem. Physics Letters *52*, 413 (1977).
[61] *G. S. Hurst, M. H. Nayfeh & J. P. Young,* Appl. Physics Letters *30*, 229 (1977).
[62] RKR program kindly supplied by *M. Stock* (University of Kaiserslautern).
[63] *C. J. Cerjan, K. K. Docken & A. Dalgarno,* Chem. Physics Letters *38*, 401 (1976).